Short-term forecasting through intermittent assimilation of data from Taiwan and mainland China coastal radars for Typhoon Meranti (2010) at landfall

Kun Zhao,[1] Xinfeng Li,[1] Ming Xue,[1,2] Ben Jong-Dao Jou,[3] and Wen-Chau Lee[4]

Received 8 November 2011; revised 5 January 2012; accepted 31 January 2012; published 29 March 2012.

[1] Radial velocity (Vr) and reflectivity (Z) data from eight coastal operational radars of mainland China and Taiwan are assimilated for the first time using the ARPS 3DVAR and cloud analysis package for Pacific Typhoon Meranti of 2010. It is shown that the vortex-scale circulations of Meranti can be adequately established after only 2 hourly assimilation cycles while additional cycles provide more details for subvortex-scale structures. Subsequent 12 h forecasts of typhoon structure, intensity, track, and precipitation are greatly improved over the one without radar data assimilation. Vr data lead to a larger improvement to the intensity and track forecasts than Z data, while additional Z data further improve the precipitation forecast. Overall, assimilating both Vr and Z data from multiple radars gives the best forecasts. In that case, three local rainfall maxima related to typhoon circulations and their interactions with the complex terrain in the southeast China coastal region are also captured. Assimilating radar data at a lower 3 or 6 hourly frequency leads to a weaker typhoon with larger track forecast errors compared to hourly frequency. An attempt to assimilate additional best track minimum sea level pressure data is also made; it results in more accurate surface pressure analyses, but the benefit is mostly lost within the first hour of forecast. Assimilating data from a single Doppler radar with a good coverage of the typhoon inner core region is also quite effective, but it takes one more cycle to establish circulation analyses of similar quality. The forecasts using multiple radars are still the best.

Citation: Zhao, K., X. Li, M. Xue, B. J.-D. Jou, and W.-C. Lee (2012), Short-term forecasting through intermittent assimilation of data from Taiwan and mainland China coastal radars for Typhoon Meranti (2010) at landfall, *J. Geophys. Res.*, *117*, D06108, doi:10.1029/2011JD017109.

1. Introduction

[2] China is one of the world's countries suffering the most from typhoon damage, and the average number of tropical cyclones (TCs) making landfall along the China coast is about nine per year, according to the Yearbook of Tropical Cyclones (typhoon) from Chinese Meteorological Administration (CMA). Accurate prediction of the track, intensity and associated precipitation of TCs making landfall can help reduce the loss of lives and property. Over the past decade, TC track forecasts have improved steadily because of the increased use of nontraditional data (e.g., satellite data) and the advancement of numerical weather prediction (NWP) models. However, TC intensity and structure forecasts have improved very slowly [*Houze et al.*, 2007]. Particularly, TCs with abrupt intensity changes are often poorly predicted by the operational models. The lack of accurate initial conditions capturing the internal structure of TCs has been attributed as one of the main factors [*Davis et al.*, 2008].

[3] Coastal Doppler weather radar is the only platform that can observe the three-dimensional structure of TCs near landfall with sufficiently high temporal (~6 min) and spatial resolutions (~1 km). How to effectively assimilate these radar data into the numerical model for the TC analysis and forecast has received great interest in recent years from TC researchers. Several recent studies assimilated radar observations into high-resolution TC prediction models to improve the initial conditions and prediction of TCs at landfall, using three-dimensional variational (3DVAR) methods [e.g., *Xiao et al.*, 2007; *Zhao et al.*, 2008; *Zhao and Jin*, 2008; *Zhao and Xue*, 2009; *Lin et al.*, 2011] or ensemble Kalman filter (EnKF) [e.g., *Zhang et al.*, 2009; *Dong and Xue*, 2010; J. Dong and M. Xue, Coastal WSR-88D radar data assimilation with ensemble Kalman filter for analysis and forecast of

[1]Key Laboratory of Mesoscale Severe Weather/MOE, School of Atmospheric Sciences, Nanjing University, Nanjing, China.
[2]Center for Analysis and Prediction of Storms and School of Meteorology, University of Oklahoma, Norman, Oklahoma, USA.
[3]Department of Atmospheric Sciences, National Taiwan University, Taipei, Taiwan.
[4]Earth Observing Laboratory, National Center for Atmospheric Research, Boulder, Colorado, USA.

0148-0227/12/2011JD017109

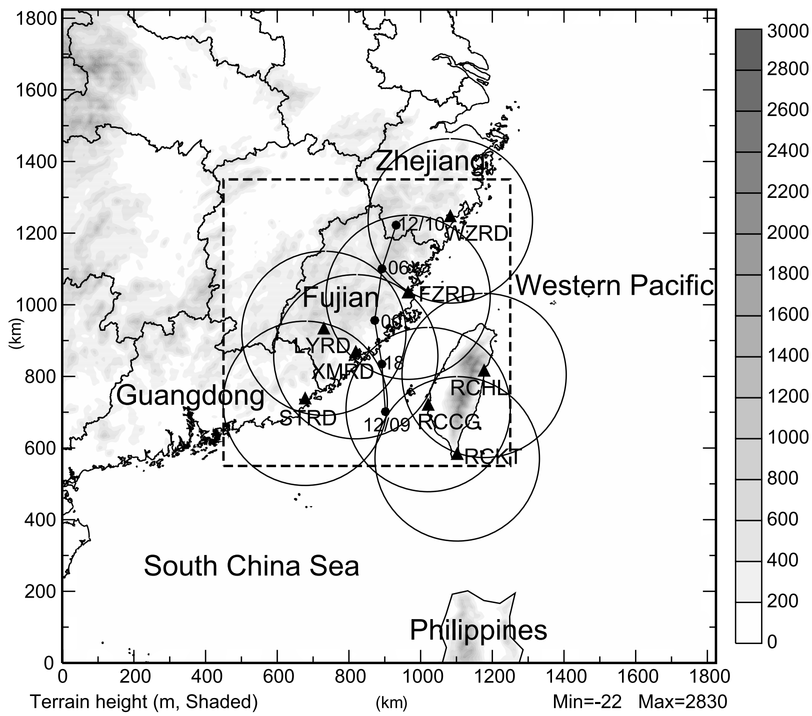

Figure 1. The analysis and prediction domain at 3 km horizontal resolution, with the best track locations of Typhoon Meranti marked at 6 h intervals from 12:00 UTC, 9 September, to 12:00 UTC, 10 September 2010. The locations of radar stations are shown by the solid triangles, and the maximum Doppler ranges of the radar data are indicated by the solid circles. The dashed square box indicates the region of the reflectivity/precipitation verification. The gray shading shows the terrain height. Radar data assimilation occurs between 12:00 and 18:00 UTC before landfall.

Hurricane Ike, submitted to *Quarterly Journal of the Royal Meteorological Society*, 2011]. Among these existing methods, an efficient and effective way to assimilate high-frequency coastal radar data is to employ intermittent assimilation cycles with a 3DVAR system combined with a mesoscale model. *Zhao and Xue* [2009] applied a 3DVAR/cloud analysis package from the ARPS modeling system [*Xue et al.*, 2003] for the first time to the initialization of a hurricane using data from two U.S. Gulf of Mexico coastal radars. This system had been demonstrated to be effective for convective storms [e.g., *Xue et al.*, 2003; *Hu et al.*, 2006a, 2006b; *Hu and Xue*, 2007], typically using frequent assimilation cycles. The results of *Zhao and Xue* [2009] show that the assimilation of radial velocity (Vr) data has more impact on the track and intensity forecast, while the assimilation of reflectivity (Z) data has more impact on the precipitation structure forecast, and can also improve the intensity forecast through moisture adjustment. *Zhao and Xue* [2009] assimilated radar data over a 6 h period at 30 min intervals. In contrast, most other TC radar data assimilation (DA) studies based on other 3DVAR systems used only one or a few analyses at longer intervals [e.g., *Xiao et al.*, 2007; *Lin et al.*, 2011], not taking full advantage of the high frequency of radar observations. While the results of the above studies are encouraging, the cases studied so far are rather few, and different TC systems may have different responses to the data as well as the DA system and methods used. Furthermore, the performance of the ARPS 3DVAR/cloud analysis system as applied to typhoon initialization in the Asian region has not been documented in published literature. In general, radar DA remains a challenging problem.

[4] With the deployment of the Chinese next generation Weather Surveillance Radar 1998 Doppler (CINRAD WSR-98D) network and the Taiwan operational radar network in recent years, effective assimilation of high-resolution data from these radars into NWP models for improving landfall of TC forecasts becomes an important issue for the local research and operational communities. This study explores for the first time the intermittent assimilation of radar data from mainland China and Taiwan within the ARPS 3DVAR/complex cloud analysis framework, for the analysis and prediction of a typhoon with sudden intensification near the coast. The typhoon to be studied is Meranti (2010), the eleventh TC of the 2010 typhoon season in the western North Pacific. Meranti formed as a tropical depression east of Taiwan on 7 September 2010 and moved southwest immediately afterward. It intensified into a tropical storm by 06:00 UTC, 8 September, then turned and moved northward. It underwent rapid intensification from 18:00 UTC, 8 September ($\sim$25.5 h prior to landfall) to 18:00 UTC, 9 September, with the peak surface wind speed increasing from 20 m s^{-1} to 35 m s^{-1} when approaching landfall according to the official best track data from CMA [*Yu et al.*, 2007]. The storm weakened rapidly after landfall (19:30 UTC) and brought heavy rainfall and strong winds to coastal Fujian and Zhejiang Provinces. The real-time forecasts by the operational Global Forecast Systems at CMA and the National Centers for Environmental

Predication (NCEP) failed to capture the intensification near the coast, or the heavy rain in Fujian.

[5] At the stage of rapid intensification, Meranti was located in the Taiwan Strait, within the range of costal radars in mainland China and Taiwan (Figure 1). These radars provided valuable three-dimensional observations of TC structure with high spatial and temporal resolution, but their data were not used in real-time operational models. This study assimilates Vr and Z data into the ARPS model [*Xue et al.*, 2000; *Xue et al.*, 2001; *Xue et al.*, 2003] and examines its performance in predicting the structure, intensity, and quantitative precipitation of Meranti. Compared to the short paper of *Zhao and Xue* [2009] that only briefly discussed the impact of radar data assimilated using a fixed cycling strategy on the final analysis and the forecast, this study examines in more detail (1) the analysis increments produced by the 3DVAR/cloud analysis system using radar data, (2) the dynamic and thermodynamic responses during the forecast step, (3) the effects of assimilation configurations on forecast, (4) the three dimensional structure of the analyzed typhoon, and (5) the amount and spatial distributions of precipitation after typhoon landfall.

[6] This paper is organized as follows. Section 2 describes radar data processing, the assimilation method, and the design of assimilation experiments. The analysis results are presented and discussed in section 3 while the prediction results are shown in section 4. The impacts of assimilation strategies on the forecast are discussed in section 5. Summary and conclusions are presented in section 6.

2. Data, Methodology, and Experimental Design

2.1. Radar Data Processing and Quality Control

[7] In this paper, radar data from eight S band coastal Doppler radars, including five CINRAD WSR-98D radars along the southeast coast of mainland China and three Gematronik 1500S Doppler radars on the Taiwan Island, are used. Specifically, these radars are located at Xiamen (XMRD), Fuzhou (FZRD), Longyan (LYRD), Santou (STRD), Wenzhou (WZRD), Ken-Ting (RCKT), Hua-Lien (RCHL), and Chi-Gu (RCCG) sites, as shown in Figure 1. All of them operated in the same volume coverage pattern 21 (VCP21) scanning mode of WSR-88D in the United States, which consists of nine elevations between 0.5° and 19.5° [*Crum et al.*, 1993]. The maximum Doppler ranges for WSR-98D and Gematronik radars are 230 km. The data quality control procedures within the 88d2arps program available in the ARPS system [*Brewster et al.*, 2005] is first used to automatically remove/correct erroneous observations, including velocity dealiasing and ground clutter removal. These data are then examined and edited manually using the NCAR "SOLO" software [*Oye et al.*, 1995]. Finally, the quality controlled data are spatially mapped onto the model grid using a local least square fitting method [*Brewster et al.*, 2005] before they are analyzed by the ARPS 3DVAR/Complex cloud analysis system. This data remapping procedure can be considered data thinning which helps reduce the analysis cost, and also has the benefit of making the uncorrelated observation error assumption more valid. Similar to most previous radar data assimilation studies, we only use Z and Vr data in regions where Z is no less than 15 dBZ. Such a threshold actually corresponds to very low values of hydrometeor mixing ratios, and the data in low-reflectivity regions usually have high noise levels because of low signal-to-noise ratio with the radar measurements.

2.2. ARPS Prediction Model and ARPS3DVAR/Complex Cloud Analysis System

[8] The nonhydrostatic ARPS prediction model with full physics is used during the assimilation cycles and for the subsequent forecast. The physics options used include the Lin ice microphysics, Goddard longwave and shortwave radiation, a 2 layer soil model and the turbulent kinetic energy (TKE)-based subgrid-scale turbulence and planetary boundary layer (PBL) parameterizations [see *Xue et al.*, 2001]. A domain of 1830 × 1830 × 25 km is used (Figure 1), consisting of 611 × 611 × 53 grid points with a 3 km horizontal grid spacing and varying vertical resolutions ranging from 50 m at the surface to 770 m at the model top. The initial analysis background and the lateral boundary conditions (LBCs) are from 6 hourly operational NCEP Global Forecast System (GFS) analyses combined with 3 h forecasts at a 0.5° resolution.

[9] The ARPS 3DVAR uses an incremental form of the cost function that includes the background, observation, and mass-continuity equation constraint terms. The analysis variables include three wind components, potential temperature, pressure, and water vapor mixing ratio [*Gao et al.*, 2004]. In the current system, the cross correlations between variables are not included in the background error covariance. The spatial covariance of background error is assumed to be spatially homogeneous and Gaussian, and is modeled using a recursive filter. The observation errors are assumed to be uncorrelated so that the observation error covariance matrix is diagonal, and its diagonal elements are specified according to the estimated observation errors. Except for the wind variables that are coupled through the mass continuity constraint, the ARPS 3DVAR is effectively a univariate analysis system; the assimilation of Vr data directly affects wind only. The standard deviation of Vr observation errors is prescribed to be 1.5 m s^{-1} similar to that used by *Zhao and Xue* [2009]. Since Vr data have been edited carefully in the objective and subjective quality control steps, the observational errors in Vr are mainly due to inhomogeneities of velocity and reflectivity within a sampling volume that generally have a standard error of about 1 m s^{-1} as the lower bound [*Doviak et al.*, 1976]. When applying the radar data, the horizontal and vertical covariance decorrelation scales are set as 10 km and 4 grid intervals, respectively. These settings are similar to those used by *Zhao and Xue* [2009] and other related studies. After the 3DVAR analysis, complex cloud analysis is performed using reflectivity data to adjust the cloud and hydrometeor fields as well as in-cloud temperature and moisture. The rainwater mixing ratio (q_r) is estimated via the reflectivity formula of *Kessler* [1969], and snow (q_s) and hail (q_h) are estimated using the reflectivity equations of *Rogers and Yau* [1989]. The cloud analysis package contains a hydrometeor classification procedure that controls the partitioning of water and ice substances among the species while ensuring the reflectivity calculated from the model state variables matches the observations. The in-cloud temperature and moisture are retrieved by assuming a modified moist-adiabatic ascent that accounts for entrainment. More details on the cloud analysis procedure can be

Table 1. List of Experiments

Experiment	Description
CNTL	No radar data assimilation
ExpV	Assimilating radial velocity only at hourly intervals
ExpVZ	Assimilating radial velocity and reflectivity data at hourly intervals
ExpVZ3h	Same as ExpVZ but with 3 hourly analysis cycles
ExpVZ6h	Same as ExpVZ but with 6 hourly analysis cycles
ExpVZRCCG	Same as ExpVZ but with data from Taiwan Chi-Gu (RCCG) radar only
ExpVZMSLP	Same as ExpVZ but with additional MSLP data from best track

found in the work of *Hu et al.* [2006a]. In this study, we do note that repeated adjustment of the in-cloud water vapor mixing ratio (q_v) via the cloud analysis procedure in the high-frequency assimilation cycles may result in unrealistic warming in the middle troposphere and too much precipitation, similar to the finding of *Schenkman et al.* [2011]. Thus, the cloud analysis procedure is modified so that q_v is adjusted only in the first analysis cycle. Sensitivity experiments showed better results with this configuration.

2.3. Experimental Design

[10] The baseline control forecast without radar DA (CNTL) starts at 18:00 UTC, 9 September, from the NCEP GFS analysis (Table 1). In other experiments, radar data are assimilated from 12:00 to 18:00 UTC, spanning the last 6 h of the rapid intensification stage. Twelve hour forecasts are then launched from 18:00 UTC, and the forecast hours cover the landfall and postlandfall periods of Meranti (Figure 1) when Meranti is weakening. The DA experiments are divided into two groups. The first group is designed to investigate the impact of assimilating Z and/or Vr data, and it includes two experiments with 1 h assimilation intervals: one with Vr only (ExpV), and one with both Z and Vr data (ExpVZ). The second group is designed to examine the impact of different assimilation configurations, including assimilation frequency (ExpVZ3h and ExpVZ6h), single radar (ExpVZRCCG) versus multiple radars, and the assimilation of additional minimum sea level pressure (MSLP) data (ExpVZMSLP). ExpVZ3h and ExpVZ6h are the same as ExpVZ except for the 3 h and 6 h assimilation intervals, respectively, as compared to 1 h in other experiments (Table 1). Experiment ExpVZRCCG uses data from RCCG radar only, which was best positioned to capture the inner core regions of Meranti (Figure 1). Considering the poor coverage of ground-based Doppler radars in the lower troposphere because of nonzero elevation, terrain blockage, and Earth curvature effect, and also the inability of the ARPS 3DVAR system to directly update pressure using radar data, we experimented with direct assimilation of additional MSLP data from the best track data in experiment ExpVZMSLP (Table 1), to see if the MSLP data can improve the analysis and forecast. The MSLP data are treated as point measurements located at the surface and at the center of the background vortex. Figure 2 shows the flow diagrams for each of the experiments.

3. Analysis Results With Radar Data Assimilation

[11] In this section and section 4, we will present and discuss analysis and forecast results from experiments ExpVZ and ExpV and compare them with experiment CNTL that did not assimilate any radar data. Data from all

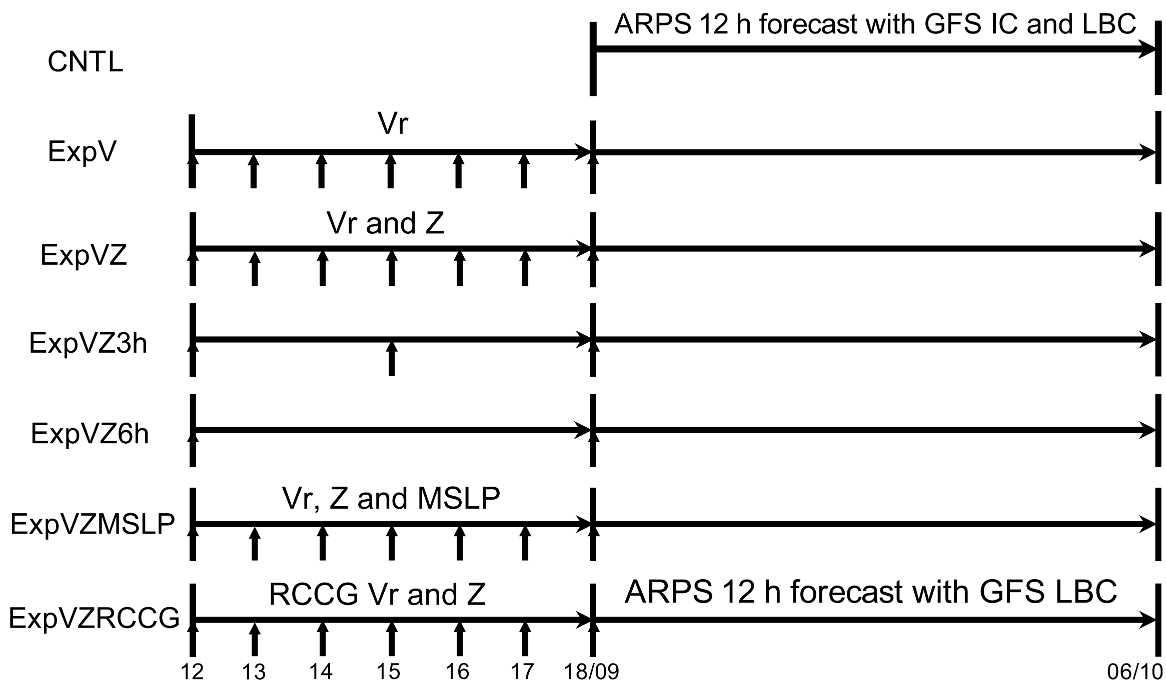

Figure 2. Flowchart of control experiment (CNTL) and experiments assimilating radar data with different configurations. Upward pointing arrows indicate the times when radar (and minimum sea level pressure (MSLP) in ExpVZMSLP) data are assimilated. A 12 h forecast follows the final analysis at 18:00 UTC, 9 September 2010 (18/09), in all experiments.

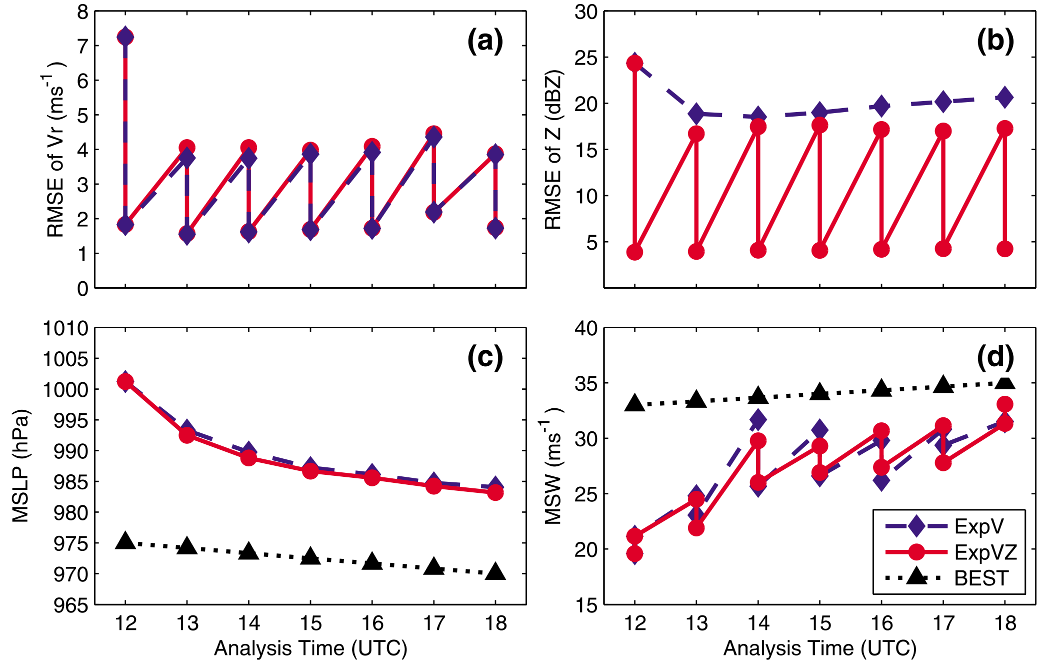

Figure 3. The root-mean-square errors (RMSEs) or observation innovations of (a) Vr and (b) Z calculated in precipitation region (dBZ >15 dBZ) and of (c) the MSLP and (d) the maximum surface wind speed (MSW) before and after each analysis from ExpV and ExpVZ. The assimilation experiments and the best track data are color coded in Figure 3d.

eight radars are used in these experiments with an assimilation interval of 1 h (Table 1). Results of sensitivity experiments will be discussed in section 5.

3.1. Analysis Innovations

[12] We first look at the impact of radar data during the assimilation cycles. The response of the model state to the data analysis and the forecast error growth through the assimilation cycles can be seen by calculating the root-mean-square differences or errors (RMSEs) of the model version of Vr, Z, MSLP and maximum surface wind (MSW) speed against radar observations and best track data. Here we use RMSE loosely for the difference between model state and observations, which also contain error. These root-mean-square differences are also called observation innovations [*Kalnay*, 2003], and in our case, the Vr and Z innovations are calculated at grid points where observed Z exceeds 15 dBZ. It is worth pointing out that the surface winds of the model forecast are from the lowest model level that is at 25 m above the surface. In this study, they are used as an approximation to the 10 m winds for comparison with the best track wind data.

[13] The innovations (RMSEs) for Vr, Z, MSLP, and MSW before and after each analysis in ExpV and ExpVZ are plotted in Figure 3, in "sawtooth" plots that are commonly used in ensemble Kalman filter DA papers [e.g., *Dowell et al.*, 2004; *Tong and Xue*, 2005]. Apparently, ExpVZ has smaller RMSEs of Z than ExpV, benefiting from the assimilation of Z data. In contrast, the RMSEs of Vr in ExpV and ExpVZ are very close, as are the MSLP and MSW, suggesting that the assimilation of Vr data has a dominant impact on the intensity analysis. The RMSEs of Vr (Z) in ExpVZ show the largest reduction in the first DA cycle (the first analysis at 12:00 UTC), with the value decreasing from 7.5 m s^{-1} (25 dBZ) to 1.8 m s^{-1} (4 dBZ) (Figures 3a and 3b). After that, the RMSEs of Vr for each analysis cycle are below generally 2 m s^{-1}, similar to the assumed observational error. The MSLP (Figure 3c) and MSW (Figure 3d) before the first analysis, i.e., in the GFS analysis background, is about 25 hPa too high and 13 m s^{-1} too weak, respectively, compared to the official best track data from CMA. With frequent assimilation of radar data, the intensity increased steadily, with the analysis error in MSLP (MSW) decreasing to 13 hPa (2 m s^{-1}) at the end of the cycles (18:00 UTC). Figure 3 also shows that the forecast error in Vr increases to around 4 m s^{-1} from around 2 m s^{-1} during the 1 h forecasts (Figure 3a), which is not bad, considering the radar data measure convective-scale structures that have fast error growth. The error in reflectivity increases from <5 dBZ to around 17 dBZ (Figure 3b) which is not considered high either. Figure 3c shows that all of the MSLP decrease was achieved during the forecast process, with the analysis having no direct impact on pressure (no drop in error at analysis times). This is because the ARPS 3DVAR is a univariate analysis system, and cloud analysis does not adjust pressure either. The minimum pressure decrease is the result of model adjustment to the analyses of wind, temperature and moisture. Partly for this reason, the error in MSLP remained relatively large (13 hPa at 18:00 UTC). In comparison, the error in MSW decreased rather rapidly through the analysis cycles, reaching about 2 m s^{-1} at the end of the cycles (Figure 3d). This is apparently because the wind fields are directly updated by the Vr observations through the assimilation.

[14] We do note here that the MSLP estimates in best track data usually have larger uncertainty than wind speed data.

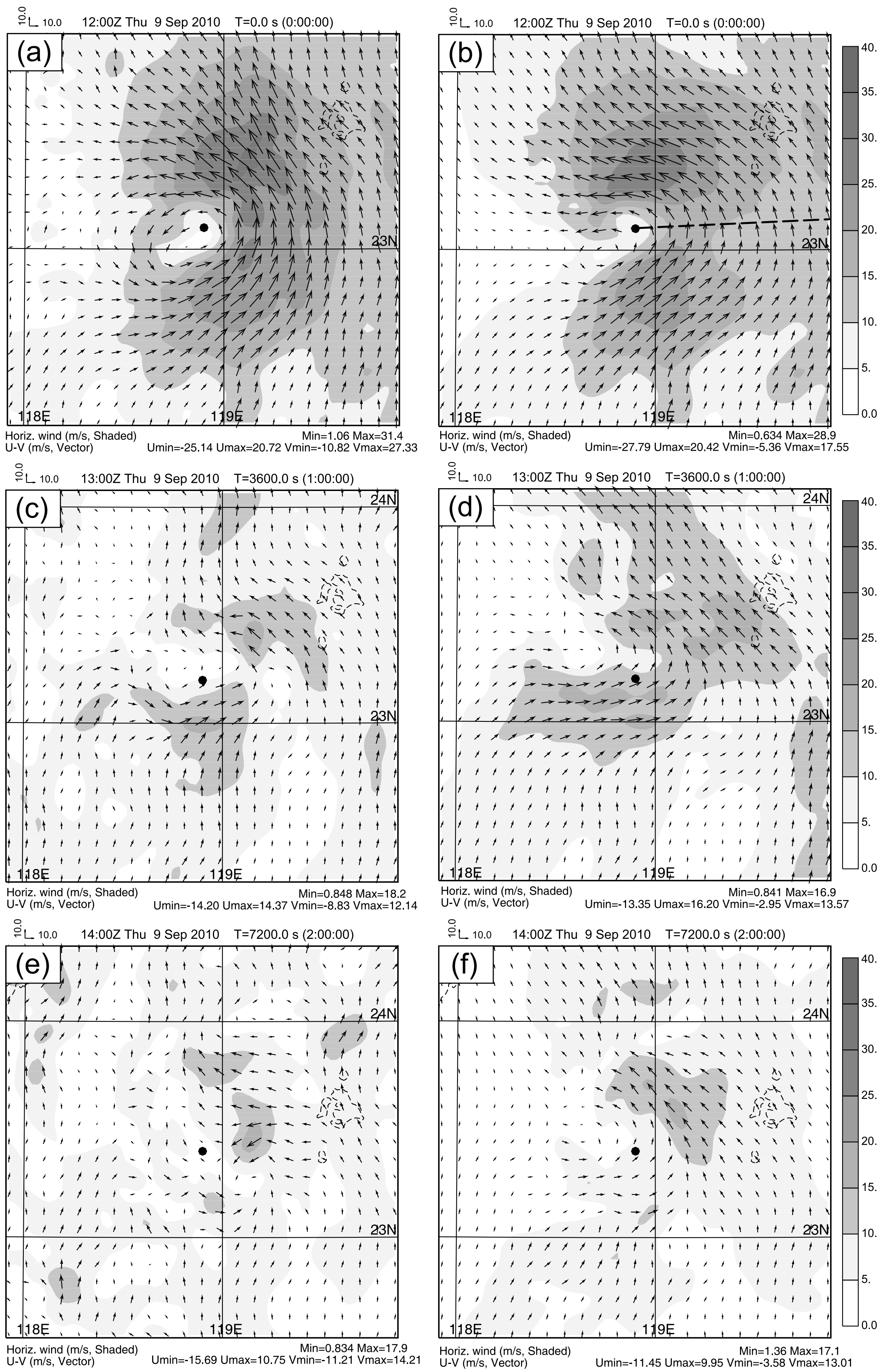

Figure 4. Horizontal wind increments at z = 3 km for (a and b) the first analysis (12:00 UTC), (c and d) second analysis (13:00 UTC), and (e and f) third analysis (14:00 UTC) from (left) ExpVZ and (right) ExpVZRCCG. The black dot indicates the approximate center location of observed typhoon.

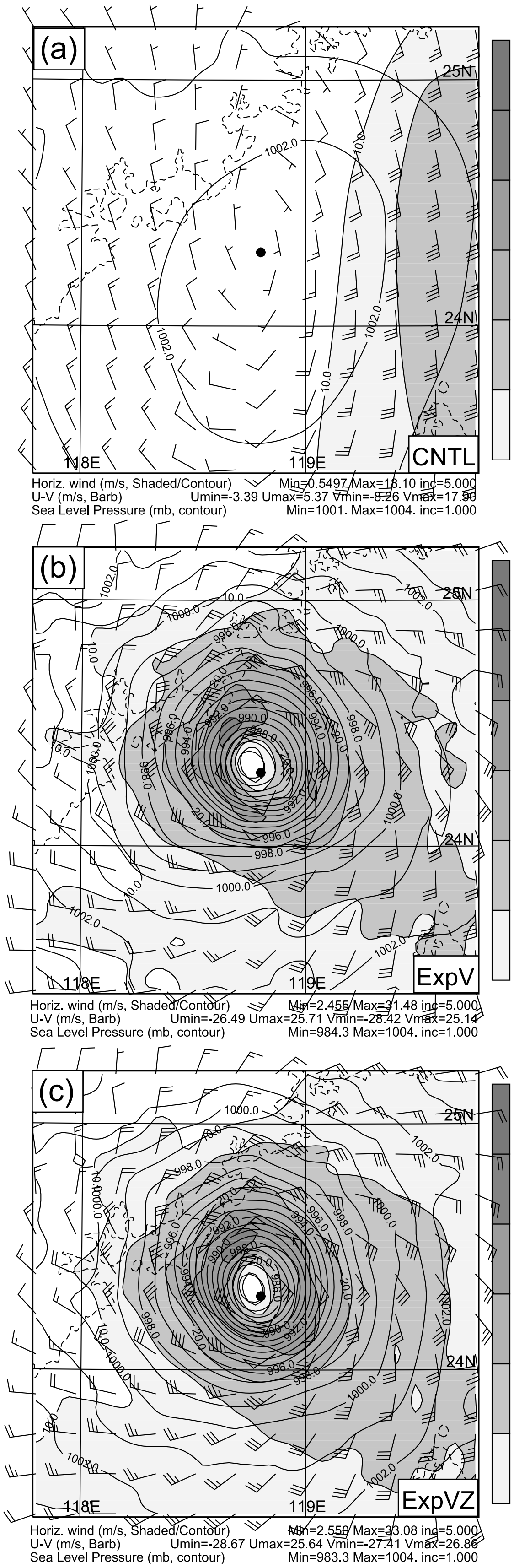

This is because MSLP is usually, as is the case of CMA best track data, estimated from estimated maximum wind speed using a wind pressure relationship [*Atkinson and Holliday*, 1977]. In the model, the surface low pressure is built up in response to the vortex circulation, in a roughly cyclostrophic balance. To see what kind of MSLP one would get from radar measured winds (which were not used for the best track estimate), we retrieved the axisymmetric tangential winds of the typhoon vortex from the Vr data of XMRD radar using the ground-based track display technique (GBVTD) [*Lee et al.*, 1999], and then estimated the MSLP using the gradient wind approximation and surface pressure measurements over land from automatic weather station [*Lee et al.*, 2000]. GBVTD was initially developed for retrieving two-dimensional primary circulations of TCs making landfall and has been shown to achieve wind retrieval accuracies of 2–3 m s^{-1} in some recent studies of mature TCs [*Lee et al.*, 2000; *Harasti et al.*, 2004; *Lee and Bell*, 2007]. The domain of the GBVTD analyses extends from the center of the typhoon to an 80 km radius and from 1 to 15 km in the vertical. At 18:00 UTC, the estimated cyclostrophic MSLP is about 980 hPa, about 10 hPa higher than the best track data (of 970 hPa). This estimate is closer to the MSLP obtained in the model (Figure 3c). To say the least, there is a larger uncertainty in the best track MSLP estimate than the wind speed estimate.

[15] It is also noted that the MSWs are reduced by the 3DVAR analysis in all except for the first and last cycles (Figure 3d), increasing the MSW error. An investigation revealed that this behavior was mainly caused by the mass divergence constraint in the ARPS 3DVAR [*Gao et al.*, 1999; *Gao et al.*, 2004] and the fact that, at the surface, there were no radar observations to directly constrain the surface wind analysis (Vr information gets spread to the surface through spatial covariance). The mass divergence constraint acts to couple the three wind components together to ensure the three dimensional mass divergence is nearly zero [*Gao et al.*, 1999; *Hu et al.*, 2006b]. The constraint also has a smoothing effect on the wind fields, which decreases the MSW. A sensitivity experiment, in which the divergence constraint was removed, showed no such decrease in MSW (not shown). Because the mass divergence constraint helps to produce more physical three dimensional wind fields, and because the TC intensity and track forecasts that include the constraint are slightly better, we choose to include it in all assimilation experiments presented in this study. The fact that wind fields do fit the Vr observations better after analysis (Figure 3a) indicates that the analysis system is generally well behaved.

3.2. Analysis Increments

[16] To better understand the behavior of radar data analysis, analysis increments in the horizontal wind components

Figure 5. Analyzed sea level pressure (SLP, thick solid contours, hPa), and surface wind speed (shaded contours, m s^{-1}) and wind barbs, for Typhoon Meranti at 18:00 UTC, 9 September 2010, from experiments (a) CNTL, (b) ExpV, and (c) ExpVZ. The black dot near the domain center indicates the approximate center location of observed typhoon.

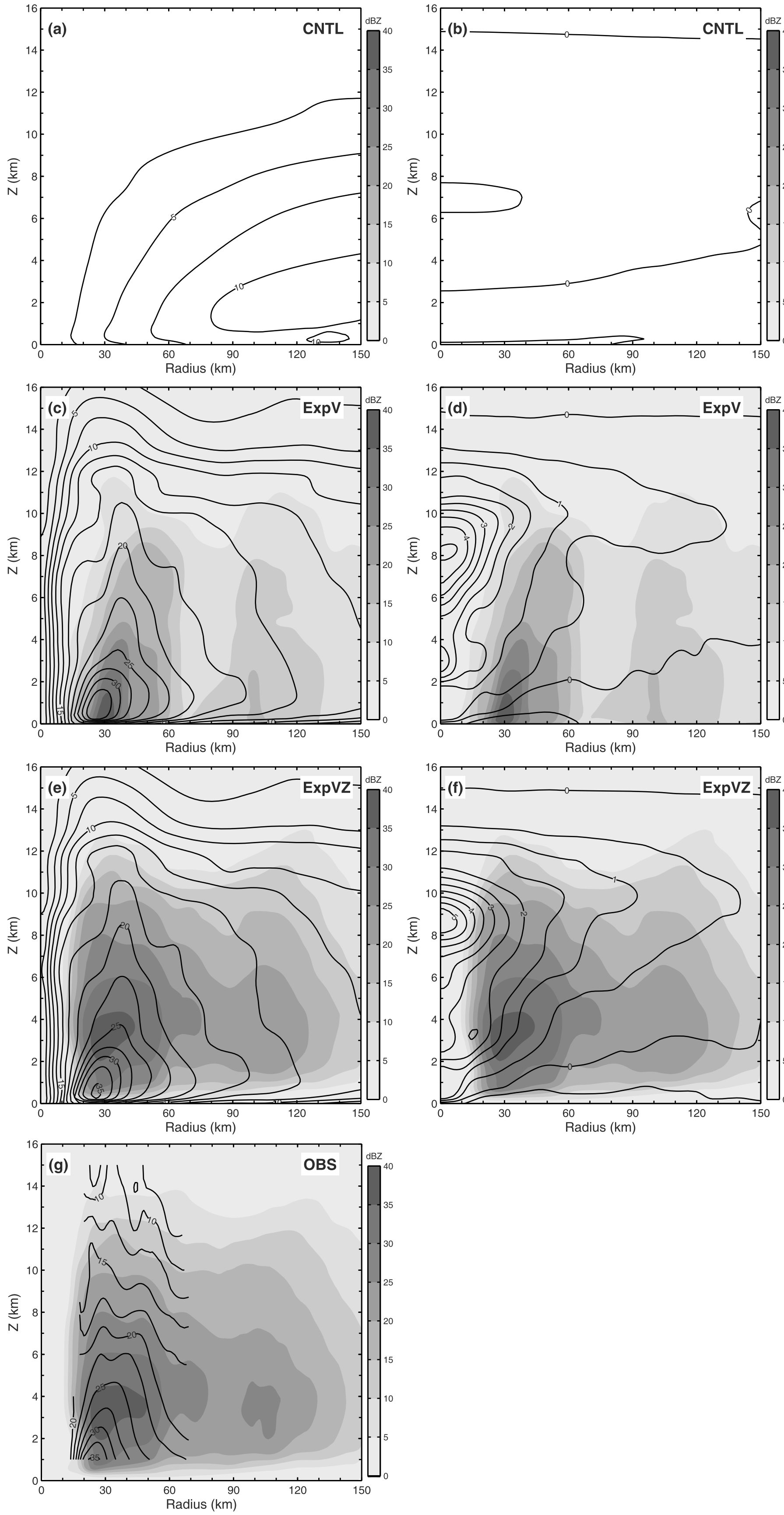
(a) CNTL
(b) CNTL
(c) ExpV
(d) ExpV
(e) ExpVZ
(f) ExpVZ
(g) OBS
Z (km)
Radius (km)
dBZ

Figure 6

at 3 km height in the first three cycles are plotted in Figure 4 for ExpVZ and ExpVZRCCG. For ExpVZ, the first analysis at 12:00 UTC produced the largest wind increments with a well-organized cyclonic structure (Figure 4a), consistent with the largest decrease in RMSE for Vr shown in Figure 3a. The clear cyclonic structure is due to the overly weak vortex in the GFS background. In the second analysis cycle (13:00 UTC), the horizontal wind increments still show a cyclonic structure, but their magnitudes are much weaker and are mainly confined to the core region (Figure 4c). By the third analysis cycle, the error in the overall vortex of the background forecast has been significantly reduced (Figure 4e) so that the wind increments are much less organized, indicating that most of the corrections correspond to structures at the subvortex scale, i.e., asymmetric structures within the typhoon vortex including those with wave number 2 and higher as well as structures related to convective rainbands. Similar structure in wind increments can be seen in the subsequent analyses (not shown). These results, together with the analysis from Figure 3, indicate that the first two cycles have the greatest impact on the vortex-scale analysis while later cycles correct mostly subvortex-scale details. At the same time, the MSLP error curve in Figure 3c suggests additional benefits of more cycles. Similar behavior is found in ExpVZRCCG (right column of Figure 4), except that a single radar is less effective in building up the vortex (more on this later).

3.3. Analyzed Typhoon Structures

[17] Figure 5 shows the sea level pressure and surface wind speed from CNTL (GFS analysis), and from ExpV and ExpVZ at the end of the DA window (18:00 UTC). Apparently, the typhoon in the GFS reanalysis is too weak (Figure 5a); its MSLP is about 1001 hPa versus 970 hPa in the best track data. The best track MSW is about 35 m s^{-1} while it is only about 18 m s^{-1} in CNTL. Meranti is significantly stronger in ExpV and ExpVZ, with the MSLP (MSW) being 984 hPa (31.5 m s^{-1}) and 983 hPa (33 m s^{-1}), respectively. The vortex circulation in ExpVZ is the strongest, with wind speeds of at least 25 m s^{-1} (second darkest shading) forming a closed circle (Figure 5c) instead of covering only the western semicircle in ExpV (Figure 5b); this is consistent with the lowest MSLP of ExpVZ. The horizontal wind speed in both ExpV and ExpVZ exhibits wave number one asymmetry with the peak winds (darkest shading) located in the northwest quadrant. Besides the improvement in intensity, the analyzed typhoon centers are closer to the observed location with radar DA. Figure 5 indicates the best track center (the black dot) at 18:00 UTC. Similar to intensity, the center locations of ExpV and ExpVZ are also very close, suggesting that the assimilation of Vr data plays a dominant role in determining the wind field and vortex circulation.

[18] To examine the vertical structure of the analyzed typhoon, the azimuthal mean tangential wind and the horizontal temperature anomaly (defined at each level as the deviation from horizontal average within a circle of 180 km radius, similar to the work of *Liu et al.* [1999]) are presented in Figures 6a–6f, for ExpV and ExpVZ, together with that of CNTL for reference. For further comparison, the azimuthal mean observed reflectivity and tangential wind retrieved from XMRD data using GBVTD [*Lee et al.*, 1999] valid at the same time are given in Figure 6g. In the GFS analysis used in CNTL, the vortex circulation is weaker and broader (Figure 6a), characterized by a large radius of maximum wind (RMW) of about 130 km, an outwardly sloping RMW axis, and a very weak warm core (Figure 6b). Since the GFS analysis contains no hydrometeors, the reflectivity field is blank in CNTL. The vortex in ExpV is much stronger with a maximum mean tangential wind speed of 33 m s^{-1} in the boundary layer and a RMW of ~30 km (Figure 6c), which are much closer to the GBVTD-retrieved values of 35 m s^{-1} and 24 km, respectively (Figure 6g). Corresponding to the stronger vortex, the maximum temperature anomaly is ~4.5°C at 8 km altitude (Figure 6d). The cycled assimilation of Vr data is also able to spin up the eye wall and eye wall rainbands, thus accurately reproducing the azimuthal mean radar reflectivity structures (Figure 6c) including a clear eye, an outward sloping eye wall with mean reflectivity exceeding 40 dBZ near R = 30 km, and an outer ring of high reflectivity near R = 100 km. These features are in general agreement with the observed azimuthal mean structures (Figure 6g), except for quantitative differences. In comparison, ExpVZ produces a slightly stronger vortex, with a 35 m s^{-1} maximum mean wind speed (Figure 6e) and a 5°C maximum temperature anomaly (Figure 6f). Benefiting from the reflectivity assimilation, the pattern and magnitude of mean reflectivity in ExpVZ are much closer to those in the observations (Figure 6g). These results are consistent with the findings of limited existing studies [*Zhao and Jin*, 2008; *Zhao and Xue*, 2009] that assimilating both Z and Vr can result in better TC circulation and precipitation structures, while assimilating Vr directly substantially improves circulation analysis. The analyzed TC structures are consistent with conceptual models of TCs.

4. Forecasting Results of ExpV and ExpZV

4.1. Impact of Radar Data on Precipitation and Structure Forecasts

[19] We first examine the forecast precipitation structures of Meranti from CNTL, ExpV and ExpVZ. Figure 7 shows the composite (column maximum) radar reflectivity and 3 km height wind fields at 3, 6, 9 and 12 h of forecast from the three experiments, as compared to observed composite reflectivity. Here, the model simulated reflectivity is calculated from the model hydrometeor mixing ratios using the same formula employed by the complex cloud analysis package. By 21:00 UTC or the 3 h forecast time, Meranti has made landfall. The observed strong precipitation is now mostly located on the northern and southwestern parts of the vortex (Figure 7a), presumably because of stronger moisture

Figure 6. (a, c, and e) Azimuthally averaged tangential wind (solid isolines with intervals of 2.5 m s^{-1}), (b, d, and f) temperature deviation from horizontal mean (solid isolines with interval of 0.5°C), and reflectivity (shaded with the scale on the right) at 18:00 UTC, 9 September 2010, from experiments (Figures 6a and 6b) CNTL, (Figures 6c and 6d) ExpV, and (Figures 6e and 6f) ExpVZ, as compared with (g) the observed mean reflectivity and GBVTD-derived tangential wind.

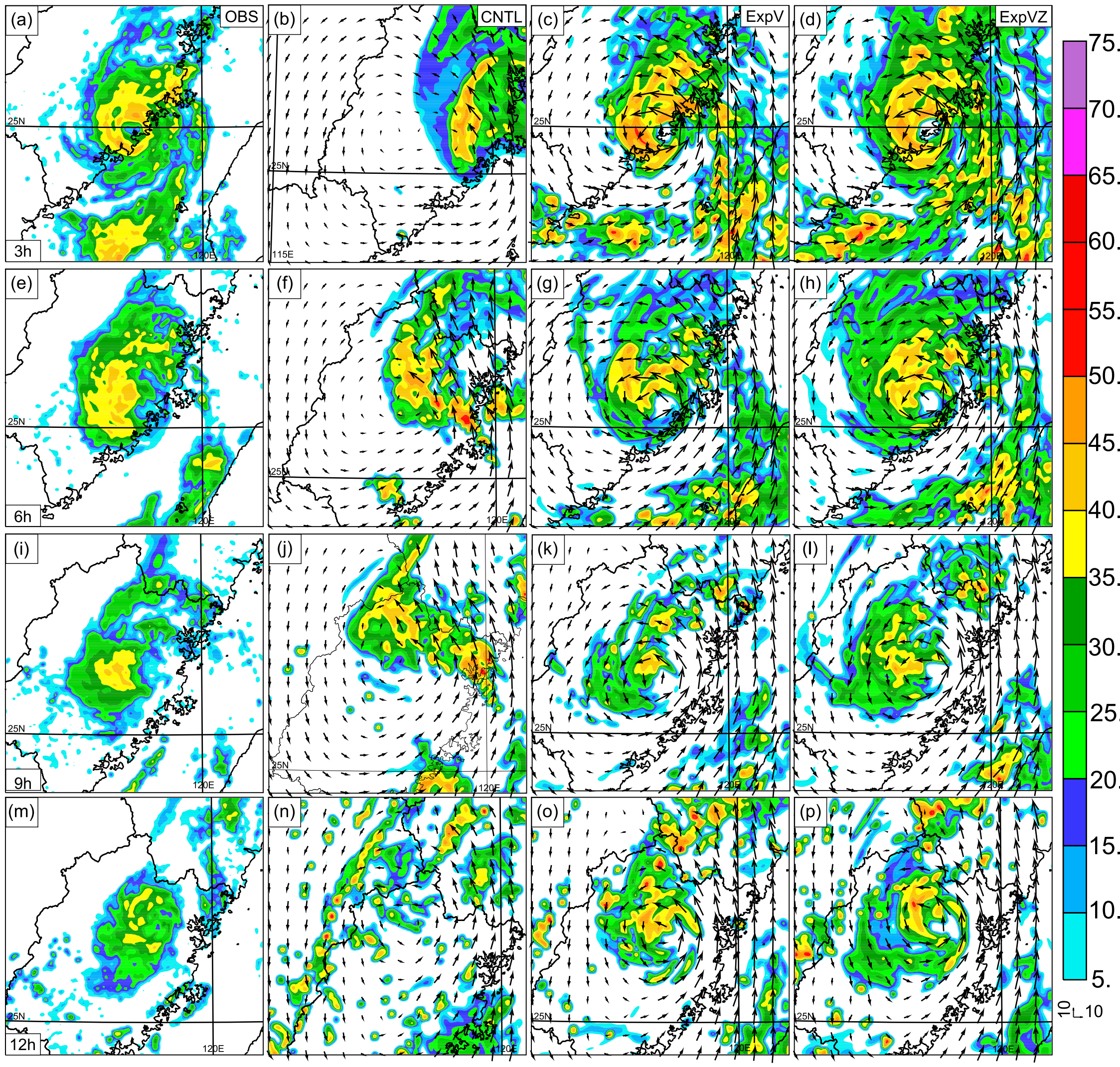

Figure 7. Observed (first column) and predicted (other columns) composite (column maximum) reflectivity and the wind vectors at 3 km MSL corresponding to (a–d) 3 h (21:00 UTC), (e–h) 6 h (00:00 UTC), (i–l) 9 h (03:00 UTC, 3rd row), and (m–p) 12 h (06:00 UTC) forecasts, from experiments CNTL (second column), ExpV (third column), and ExpVZ (fourth column).

transport from the ocean on the east side and interaction with coastal terrain in Fujian Province. The predicted vortex in CNTL (Figure 7b) is much weaker and broader than the observation and that of other experiments, as was the case at the initial condition time (compare Figure 5). The stronger circulation is not well organized in the inner core region, and the precipitation region to the south over the ocean is absent (Figure 7b). As Meranti's motion in CNTL appears faster than the observation, its center has moved to about 60 km north of the observed center. On the other hand, experiments ExpV (Figure 7c) and ExpVZ (Figure 7d) predict much better TC positions, tighter vortex circulations and well-organized eye walls, together with a small, weak reflectivity hole in the eye. Moreover, the rainband over the ocean is also captured to some extent. ExpV overpredicts reflectivity west of the center in the coastal area (Figure 7c), while ExpVZ does a better job predicting both distribution and magnitude of reflectivity (Figure 7d). By 00:00 UTC, 10 September, the precipitation pattern became more asymmetric (Figure 7e) with strong precipitation mostly found in the west half of the vortex; the observed typhoon eye more or less disappeared by this time. The TC center in CNTL has moved farther inland compared to the best track and its echo pattern does not match the observation well (Figure 7f). In contrast, ExpV and ExpVZ continue to predict strong circulations, better TC positions, and better organized reflectivity structures (Figures 7g and 7h). Visually, the regions with reflectivity exceeding 35 dBZ (yellow areas) in ExpVZ match the observations better than in ExpV, which is consistent with quantitative evaluations to be shown later. A significant difference from the observation is that both ExpV and ExpVZ still maintain a precipitation-free eye at this time, and that in ExpVZ is even present by the end of 12 h forecast. These are signs that the predicted Meranti is not filling as fast as the observed one. Such discrepancies can be due to errors in the prediction model, such as those related to the surface flux and microphysics parameterizations, as well as errors in the

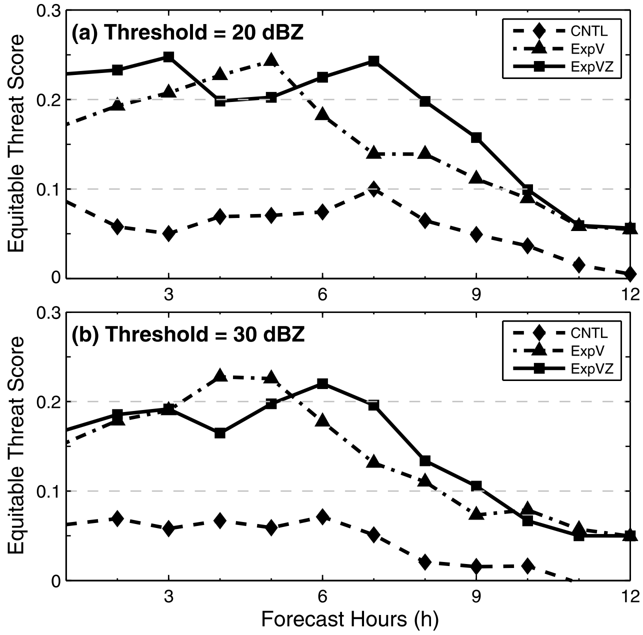

Figure 8. Equitable threat scores of predicted composite reflectivity for (a) 20 dBZ and (b) 30 dBZ thresholds from experiments CNTL, ExpV, and ExpVZ.

initial condition. An investigation of the exact cause is beyond the scope of this paper.

[20] At the 9 h forecast time, the observed precipitation pattern became even more asymmetric (Figure 7i). The observed reflectivity structure is again best captured by ExpVZ (Figure 7l). The reflectivity in CNTL becomes disorganized (Figure 7j). The reflectivity pattern in ExpV is closer to observations than in CNTL, but the reflectivity west of the vortex center is a little too weak, while those to the north are overpredicted (Figure 7k). The vortex circulations in ExpV and ExpVZ are close, and still appear tighter than in CNTL. At the 12 h forecast time, precipitation has weakened considerably and stronger echoes remain on the west half of the vortex (Figure 7m). Again, ExpVZ predicts the best reflectivity structures (Figure 7p), while CNTL performs the worst compared with observations (Figure 7n); in fact, no clear vortex structure is seen in the CNTL prediction.

[21] For quantitative evaluation of forecast precipitation, equitable threat scores (ETS, also called Gilbert Skill Score [*Schaefer*, 1990]) of instantaneous composite radar reflectivity at 20 and 30 dBZ thresholds are calculated for different forecast ranges for the three experiments (Figure 8). The observed composite reflectivity fields were constructed from level II data from multiple radars, some of which were shown earlier in Figure 7. For the 20 dBZ threshold, CNTL has the lowest scores in the entire 12 h of forecast (Figure 8a), with values <0.1. ExpVZ shows the highest scores at all times except for 4 and 5 h. The scores of ExpVZ are about 0.2 in the first 8 h then decrease rapidly to below 0.1 after 10 h; the weakening of precipitation after landfall is at least partially responsible for the rapid reduction. Similar characteristics of scores can also be seen for the 30 dBZ threshold (Figure 8b). These scores indicate that the assimilation of Z in addition to Vr further improves precipitation forecast while the assimilation of Vr data alone is also quite effective. These quantitative ETSs are consistent with our earlier subjective assessment of precipitation structures.

4.2. Track and Intensity Predictions

[22] The predicted typhoon tracks, MSW and MSLP from CNTL, ExpV, and ExpVZ are plotted in Figure 9 together with the best track for the 12 h forecast period from 18:00 UTC, 9 September, through 06:00 UTC, 10 September 2010. Figure 9a shows the predicted and observed tracks, while Figure 9b shows the track errors (in km) at each forecast hour. In CNTL, the predicted typhoon moves northward much faster than the best track (Figure 9a), resulting in a 12 h mean track error of about 92 km (Figure 9b). With the assimilation of radar data, the 12 h mean track error is reduced to 11 km and 9 km in ExpV and ExpVZ, respectively (Figure 9b). This indicates that the assimilation of radar data also has an impact on the track forecast. Such improvement in the Meranti case can be attributed to the improved vortex intensity and structure, while the large-scale environmental conditions remained about the same because of the lack of other observations in our assimilation. Note that the tracks of ExpV and ExpVZ are very close, suggesting that the assimilation of Z data has a small impact on the track forecast, similar to the results of previous studies [*Zhao and Jin*, 2008; *Zhao and Xue*, 2009].

[23] The best track MSLP and MSW and those predicted by CNTL, ExpV and ExpVZ are plotted in Figures 9c and 9d. Clearly, CNTL did not have a realistically strong vortex at the initial time, so the storm remained very weak with little MSLP change throughout the forecast. A total increase (decrease) of 25 hPa (15 m s^{-1}) in MSLP (MSW) is observed in the 12 h period, but the MSLP in CNTL changed by only a few hPa. With improved initial intensity in the radar assimilation experiments (compare Figure 3), the intensity forecast errors are much lower. In general, the predicted MSLP and MSW are similar in ExpV and ExpVZ. The predicted MSWs are within a few meters per second from the best track data throughout the forecasting hours (Figure 9d) with the decreasing trend, while the MSLPs started about 13 hPa too high (for possible reasons discussed in section 3) and became very close to the observed MSLP at the end of 12 h. These results again show the benefit of assimilating radar data. An additional experiment that assimilated reflectivity data only showed much smaller improvement (not shown). We do note again here that in our cycled cloud analysis, we do not adjust the moisture field except for the first cycle, which limits the impact of Z data. In the work of *Zhao and Xue* [2009], when moisture adjustment is performed in every cycle, Z data were found to have the largest impacts.

4.3. Precipitation Forecasting After Landfall

[24] Inland flooding is a major hazard of TCs making landfall, thus accurate precipitation forecasting near and after landfall is very important for warning purposes. Figure 10 shows the 6 h accumulated precipitation fields valid at 00:00 UTC and 06:00 UTC, 10 September, which represents periods during and after landfall, respectively, from CNTL, ExpV and ExpVZ, as compared to automatic weather station rainfall observations (first column of

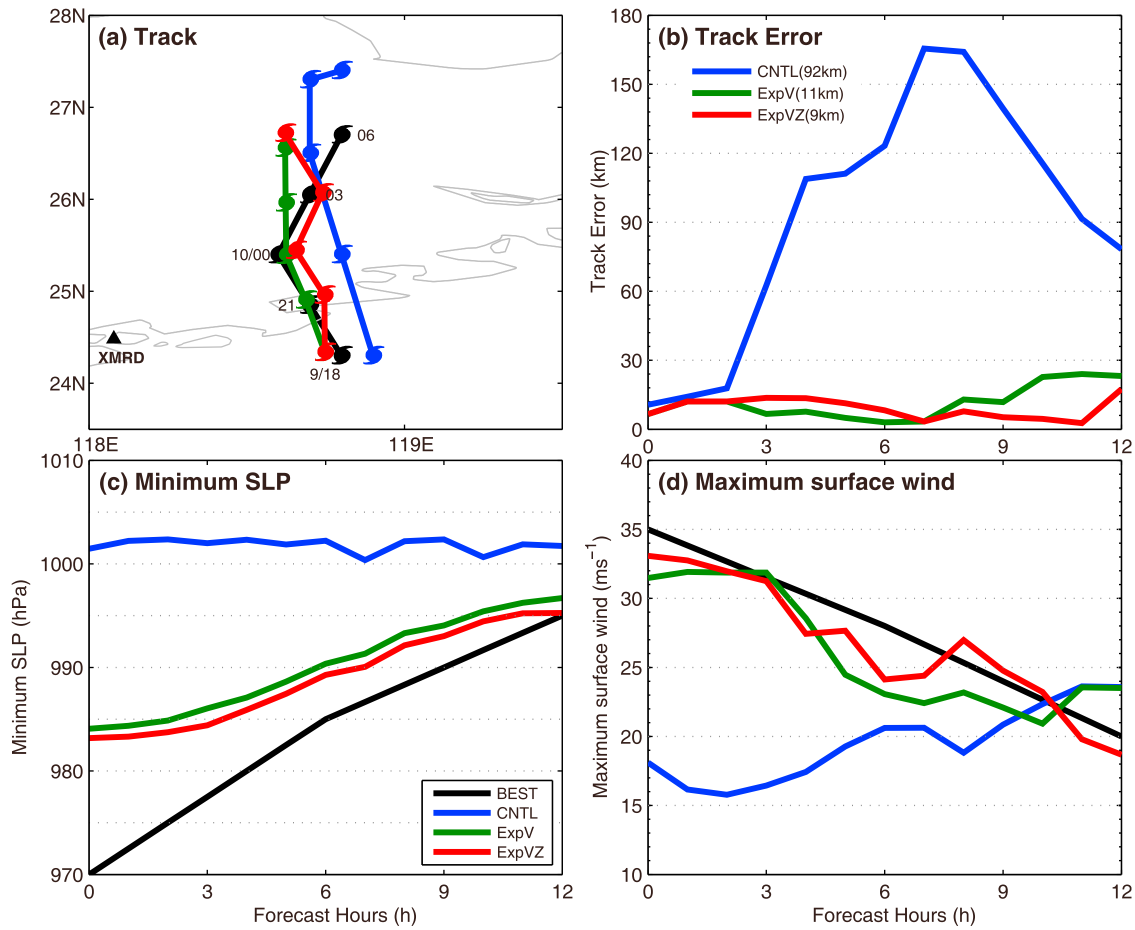

Figure 9. The 12 h predicted (a) tracks, (b) track errors, (c) MSLP (hPa), and (d) MSW (m s^{-1}) of Typhoon Meranti from 18:00 UTC, 9 September, through 06:00 UTC, 10 September 2010. Results from different assimilation experiments and the best track centers are color coded as shown in Figure 9c. Solid triangles indicate the locations of coastal radars in China. The numbers in Figure 9b represent the mean track errors over the 12 h forecast period.

Figure 10). The observations show a heavy precipitation band extending from the southeast coast to the northern mountainous areas of Fujian Province during landfall (Figure 10a). Embedded within are two heavy precipitation regions, with the strongest one extending from Shiniu Mountain (SN) to the southern mountainous area (circle A), and a weaker one at the southern coast (circle B). The maximum precipitation amount associated with region A is over 204 mm, located in a valley (118.3°E, 25.6°N) to the south of SN, which may be partly due to the valley channeling effect. After landfall (Figure 10e), the whole precipitation band moved north with the TC, producing a region of high precipitation (circle C in Figure 10e) over SN and Baiyan Mountain (BY). On the basis of the strong correlation between high precipitation and high terrain seen from Figure 10e, we suspect that terrain lifting played an important role.

[25] It is clear that CNTL forecasts the precipitation pattern and amount (Figures 10b and 10f) rather poorly. Particularly, it does not reproduce high precipitation areas A and B during landfall (Figure 10a), or C after landfall (Figure 10e). The northward bias in the precipitation location can be attributed to the excessively fast TC movement. Compared with CNTL, the two radar-assimilating experiments show significant improvements. At a glance, both ExpV (Figures 10c and 10g) and ExpVZ (Figures 10d and 10h) correctly reproduce high-precipitation regions A, B and C. Compared to rain gauge observations, the rainfall in regions A and C is generally underpredicted, while that in B is overpredicted. A careful examination indicates that ExpVZ produces a better forecast for the structure and maximum center location of the high-precipitation areas. It produces the precipitation maxima of about 100 mm over the eastern (windward) slopes of SN and the southern mountainous area of SN (Figure 10d), while ExpV only predicts a maximum of about 75 mm for the latter region (Figure 10c). Note that both experiments miss the maximum center in the valley, south of SN. This may be due to the still coarse (3 km) resolution of the model, which may not be adequate to resolve the local terrain forcing accurately. ExpVZ also decreases the overprediction of precipitation in region B, and thus produces weaker precipitation than ExpV. As for precipitation region C, ExpVZ reproduces a north-south oriented high rainband that roughly matches observations

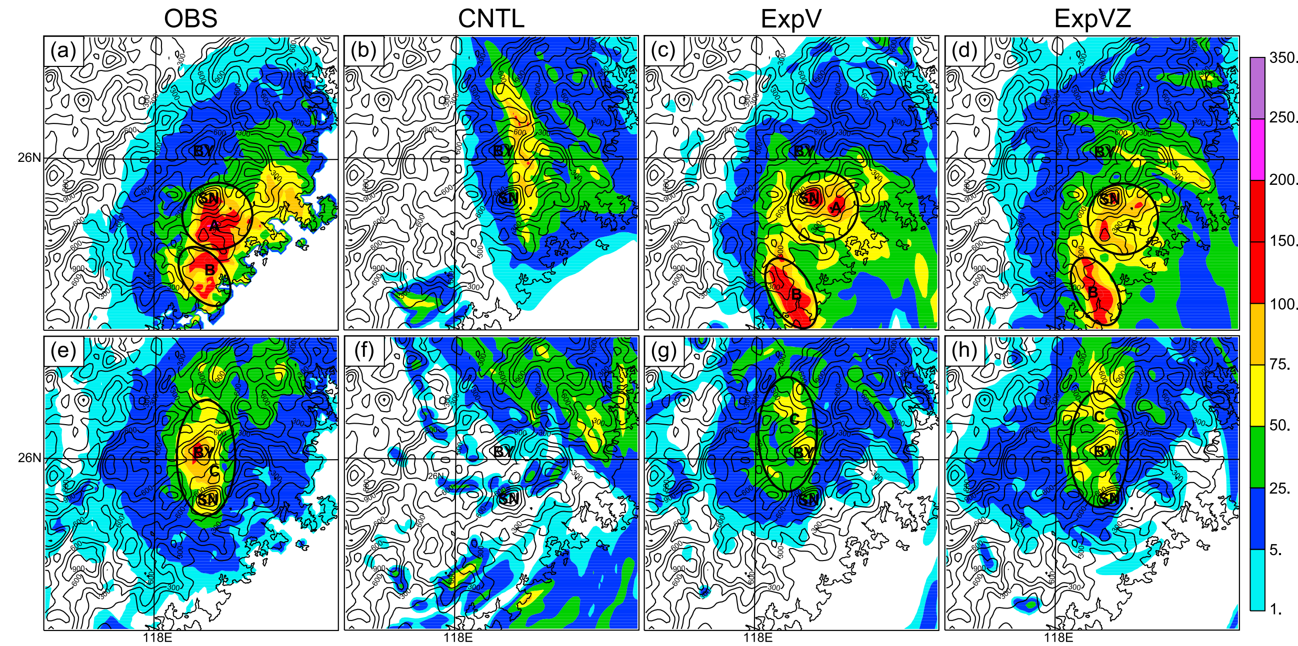

Figure 10. Six hour accumulated precipitation (mm) valid at 00:00 UTC (first row) and 06:00 UTC (second row) on 10 September 2010 from (a and e) automatic weather station hourly observations, experiments (b and f) CNTL, (c and g) ExpV, and (d and h) ExpVZ. Terrain height is indicated by contours with an interval of 150 m (MSL). Locations of Shiniu (SN) and Baiyan (BY) mountains are marked.

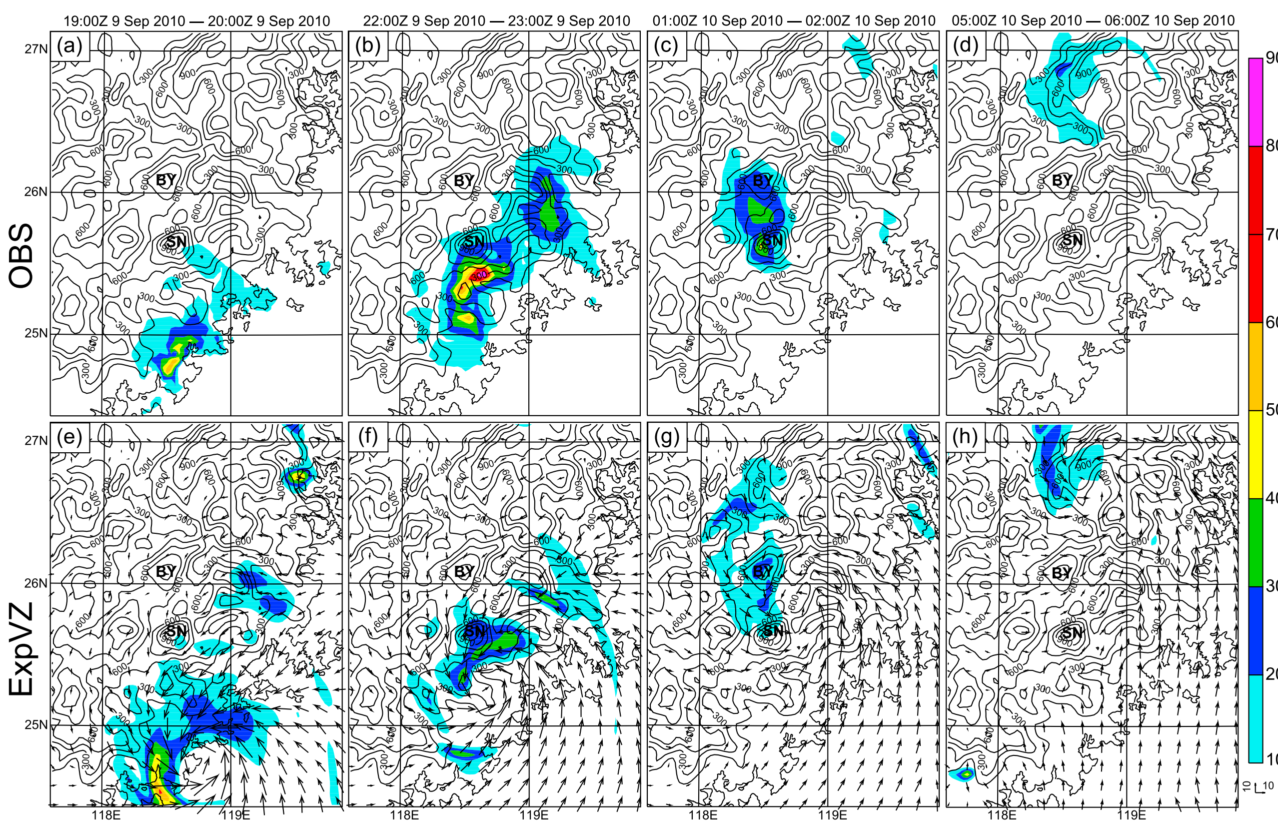

Figure 11. One hour accumulated precipitation (color shaded, mm) at (a and e) 20:00 UTC, (b and f) 23:00 UTC, 9 September, (c and g) 02:00 UTC, and (d and h) 06:00 UTC, 10 September 2010, from automatic weather station observations (first row) and experiment ExpVZ (second row). Terrain height is indicated by contours with an interval of 150 m (MSL).

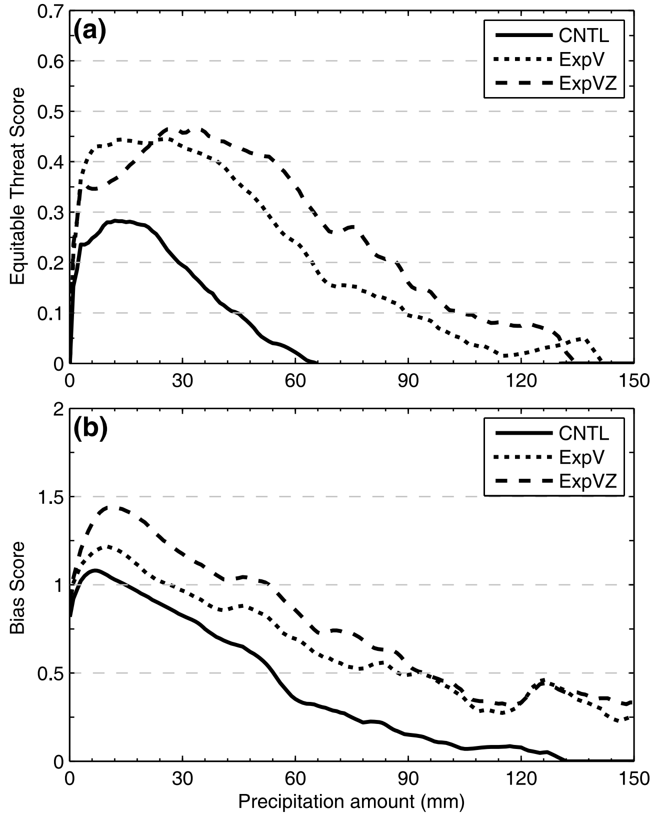

Figure 12. (a) Equitable threat scores and (b) bias scores of the 12 h accumulated precipitation forecasts from CNTL, ExpV, and ExpVZ (as shown in Figure 10), verified against automatic weather station hourly precipitation observations, valid at 06:00 UTC, 10 September 2010.

(Figure 10e), and two maximum centers over SN and BY (Figure 10h). The predicted maxima of about 50 mm in these two centers are weaker than the observed 100 and 75 mm. In comparison, ExpV predicts a maximum of about 25 mm over SN (Figure 10g).

[26] To further evaluate the spatial and temporal accuracy of forecast precipitation during and after landfall, we present in Figure 11 hourly accumulated precipitation from ExpVZ valid at 20:00 and 23:00 UTC of 9 September and at 02:00 and 06:00 UTC of 10 September, and compare them with the automatic weather station observations. At 20:00 UTC, the typhoon center had just moved across the shoreline. A precipitation band formed along the coast (Figure 11a, note that there is no precipitation observation coverage off the coast), which is reasonably well forecasted by ExpVZ (Figure 11e). This rainband should have mainly resulted from the eye wall precipitation, as shown in Figure 7a. With the northward movement of Meranti, a northeast-southwest-oriented strong precipitation band formed south of SN with the maximum located in the valley (Figure 11b), implying valley channeling effects. ExpVZ captures the banded structure, but with some position errors and a significant underestimation of amount (Figure 11f). The predicted band is displaced northward by about 10 km, thus placing the heaviest precipitation on the southeastern slope of SN instead of in the valley. The maximum precipitation in ExpVZ is about 30 mm, weaker than the observed 80 mm. An error in the typhoon track forecast can easily cause this precipitation displacement error.

[27] After 23:00 UTC, the precipitation band moved further northward with the typhoon. The heaviest precipitation is located between SN and BY at 02:00 UTC (Figure 11c), and to the northern mountainous area of BY at 06:00 UTC (Figure 11d). Overall, ExpVZ captures these precipitation regions and their evolution rather accurately except for some underestimation over SN (Figures 11g and 11h). These results indicate that assimilating Z and Vr into a TC making landfall is able to give short-range forecasts of hourly precipitation with impressive temporal and spatial accuracy. We note there have been few studies [e.g., *Hendricks et al.*, 2011] showing similarly detailed verification of precipitation within a TC making landfall that also involve complex terrain interactions.

[28] Given the availability of high-resolution precipitation data, we calculated ETSs and biases of the 12 h accumulated precipitation as a function of precipitation threshold for the three experiments (Figure 12). It is clear that the radar assimilation experiments obtain much higher ETS scores than CNTL. Among them, ExpVZ has the highest ETS score and least precipitation bias for all thresholds except for those between 5 and 30 mm. CNTL underpredicts precipitation in all categories, especially above 65 mm, consistent with a weaker predicted typhoon; its ETS scores drop quickly above the 30 mm threshold. ExpV underpredicts the precipitation for all except for the smallest thresholds (<20 mm). These quantitative scores again indicate that assimilating both Z and Vr data is advantageous in general.

5. Sensitivity Experiments

[29] Past studies have shown the importance of different radar DA strategies on the analysis and forecast of continental convective storms [e.g., *Hu and Xue*, 2007; *Xiao and Sun*, 2007]. Here, we would like to see if the positive impacts of radar data found in the previous sections are dependent on the assimilation strategy, including the assimilation cycle length, the number of radars used, and the inclusion of additional MSLP data. A set of sensitivity experiments are performed to examine these issues. For brevity, we present only the final analysis and predicted intensity and track results from these experiments.

5.1. Impact of Assimilation Interval

[30] We examine the impact of radar DA frequency in experiments ExpVZ3h and ExpVZ6h, which are the same as ExpVZ except for the use of 3 hourly and 6 hourly assimilation intervals, respectively. With the increase of assimilation interval and reduction of radar data assimilated, the analyzed typhoon is significantly weaker (Figures 13a and 13b), with the resulting MSLPs (MSWs) being 988 hPa (27.6 m s^{-1}) and 992 hPa (26.9 m s^{-1}), versus 983 hPa (33 m s^{-1}) in ExpVZ. There is also a southward error in the analyzed typhoon center location. ExpVZ6h has larger intensity and position errors of about 22 hPa and 25 km. Consistently, ExpVZ6h also has larger errors in intensity and track forecasts compared to ExpZV and ExpZV3h (Figure 14). Its mean track and intensity errors are about 14 km and 7 hPa (2.8 m s^{-1}). It is worth pointing out that, although the MSLP of ExpVZ3h is 5 hPa higher than that of

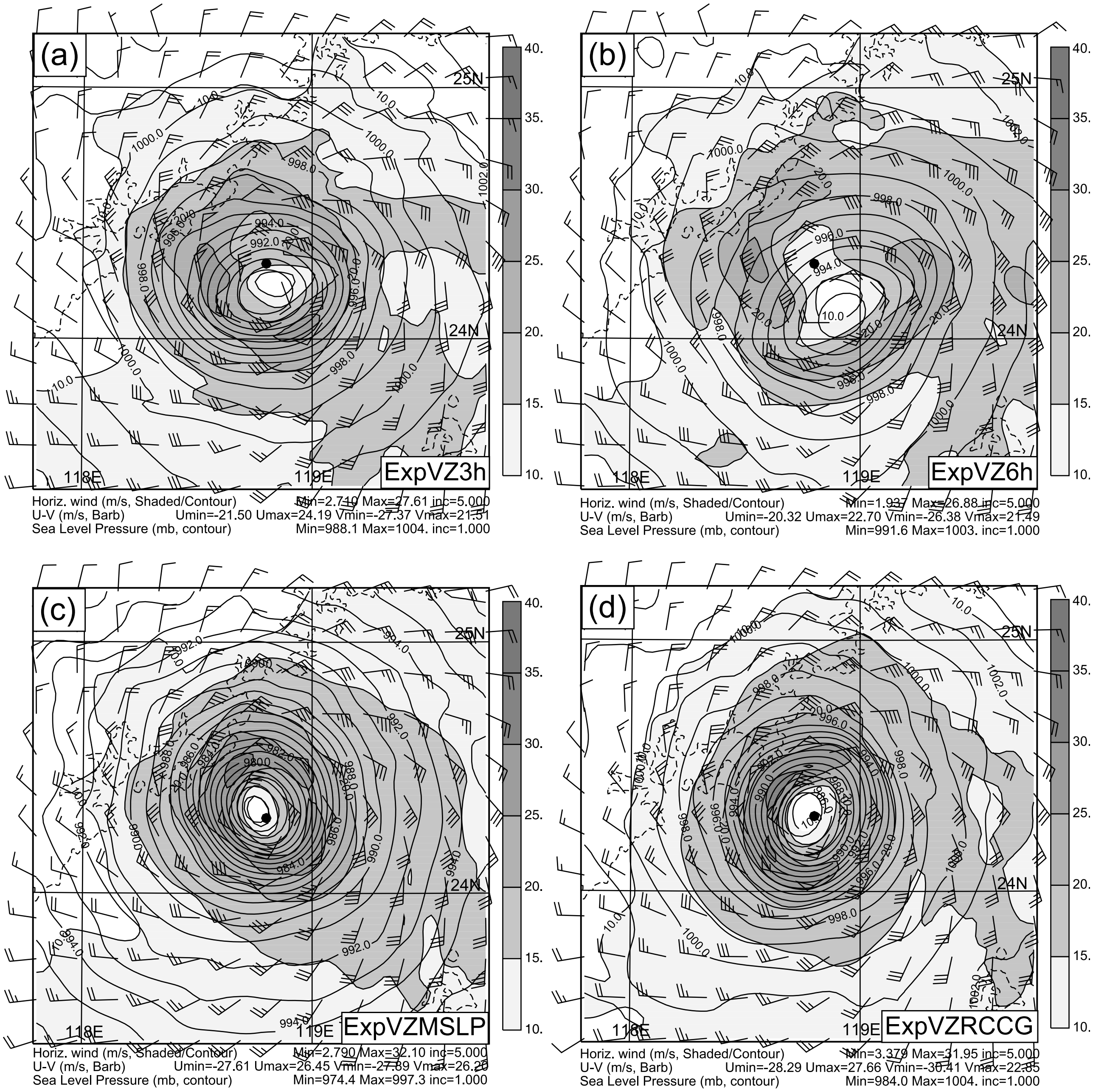

Figure 13. Same as Figure 5 but for experiments (a) ExpVZ3h, (b) ExpVZ6h, (c) ExpVZMSLP, and (d) ExpVZRCCG.

ExpVZ in the initial field, it decreases rapidly to be within 2 hPa of ExpVZ in the first hour of forecast (Figure 14c); this is apparently due to the model response to the improved circulation by radar DA. After that time, the MSLP in ExpVZ3h remains close to that of ExpVZ. A similar behavior with MSLP is found with ExpVZ6h, though the errors are larger. The MSW errors from ExpVZ3h and ExpVZ6h are larger than those of ExpVZ (Figure 14d), but still much smaller than those of CNTL shown in Figure 9c. The same is true for track error (Figures 14b and 9b). These results suggest that the higher assimilation frequency can produce better analyses and forecasts of TCs, but when radar data are only available at large time intervals, as is the case with airborne radar data, positive impacts can also be observed when the data is properly assimilated.

5.2. Impact of Assimilating MSLP Data

[31] A few recent studies [e.g., *Chen and Snyder*, 2007; *Hamill et al.*, 2011] have shown that the assimilation of best track MSLP information, as part of the so-called TC-Vitals data, can improve TC predictions. Those two studies used the more sophisticated ensemble Kalman filter [*Evensen*, 2003] method that utilizes ensemble-derived flow-dependent covariance information. In the ARPS 3DVAR, MSLP is used to update pressure only. As shown in Figure 9b, the analyzed MSLP in ExpVZ is more than 10 hPa

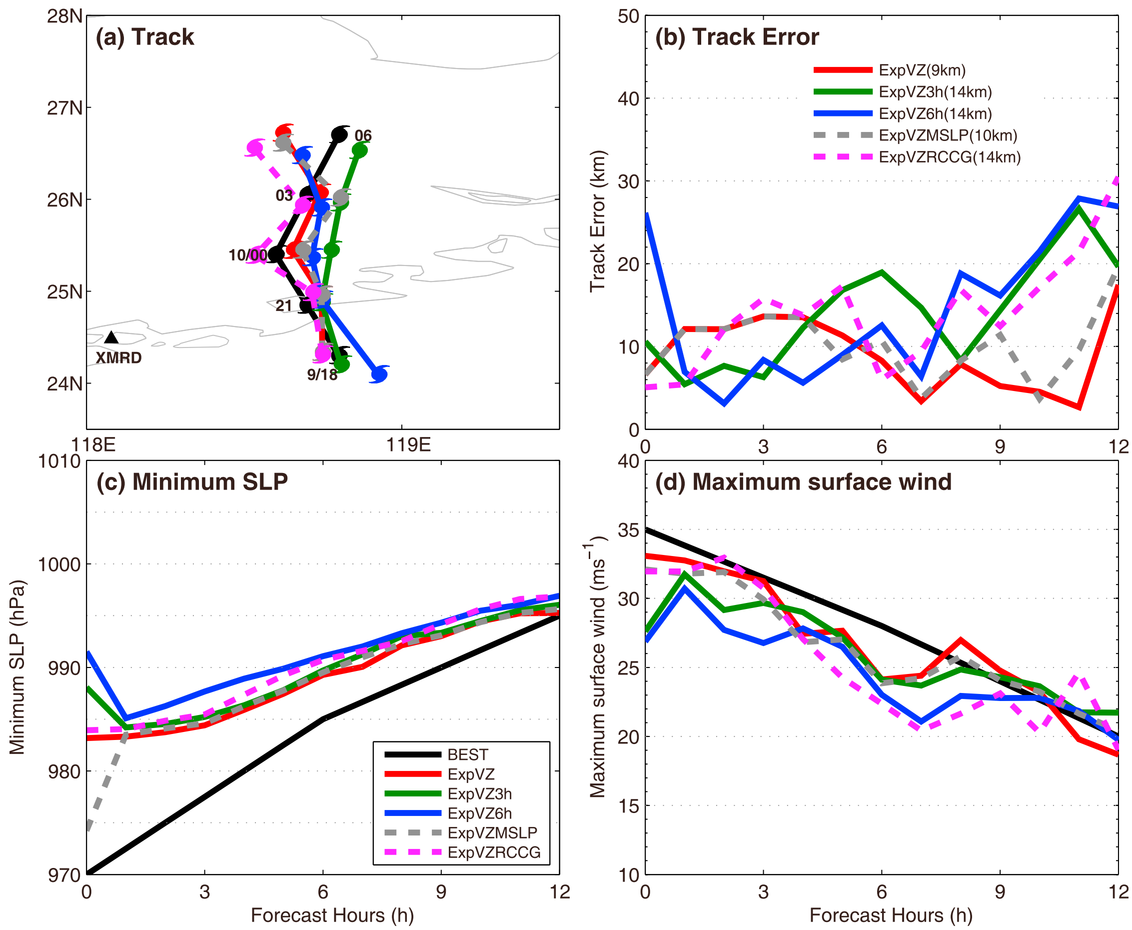

Figure 14. Same as Figure 9 but for sensitivity experiments ExpVZ3h, ExpVZ6h, ExpVZMSLP, and ExpVZRCCG, plus ExpVZ.

higher than the observed (best track) value (see also Figure 3c). Even with the uncertainty in the best track MSLP data (as discussed earlier), the analyzed MSLP is most likely too high. To see if directly analyzing MSLP data in our assimilation framework can produce further improvement, experiment ExpVZMSLP is conducted, which is the same as ExpVZ except for the addition of MSLP data. The MSLP data from the best track are first interpolated to hourly intervals between 1200 and 1800 UTC and then assimilated as single surface observations located at the best track TC center, together with the radar data through ARPS 3DVAR. In this study, a 200 km horizontal covariance decorrelation scale and a 2 hPa observation error are used for the MSLP data in the 3DVAR. The sea level pressure and surface wind speed in the final analysis are plotted in Figure 13c. Many aspects of the analyzed typhoon in ExpVZMSLP (Figure 13c) are similar to those of ExpVZ (Figure 5c), with the main differences being in the minimum pressure (Figure 14c). The analyzed MSLP in ExpVZMSLP is within 4 hPa from the best track estimate. The impact of the MSLP data on the intensity forecasting is, however, very limited. Figure 14c shows that the difference in MSLP between ExpVZ and ExpVZMSLP is mostly lost after the first hour of forecast. This is not very surprising because of the univariate nature of the ARPS 3DVAR, and the lack of temperature and wind analysis increments that balance the MSLP-derived pressure increments. Without the basic hydrostatic balance between temperature and pressure for the larger-scale pressure increments, pressure quickly adjusts to the temperature fields in the model prediction through mostly acoustic adjustment processes; in fact, most of the adjustment happens within the first 10 min of the forecast, seen by monitoring the surface pressure time tendency. To more fully realize the benefit of MSLP data, multivariate analysis methods such as EnKF and 4DVAR will be needed. This result is nevertheless worth documenting.

5.3. Impact of Single Versus Multiple Radars

[32] Our study benefits from the availability of data from multiple radars, some of which have overlapping dual-Doppler coverage. A question one can ask is how well a single, well-positioned radar can do. In our case, the RCCG radar on the southwest coast of Taiwan covered most of the inner core region of Meranti during the assimilation period (Figure 1 and 15). Experiment ExpVZRCCG is therefore performed, which is the same as ExpVZ but uses data from RCCG only. The analysis increments of horizontal winds at 3 km height in the first three cycles are shown in the right column of Figure 4 for easier comparison with ExpVZ. Similar to ExpVZ, ExpVZRCCG produces an increment of cyclonic circulation around the observed TC center in its

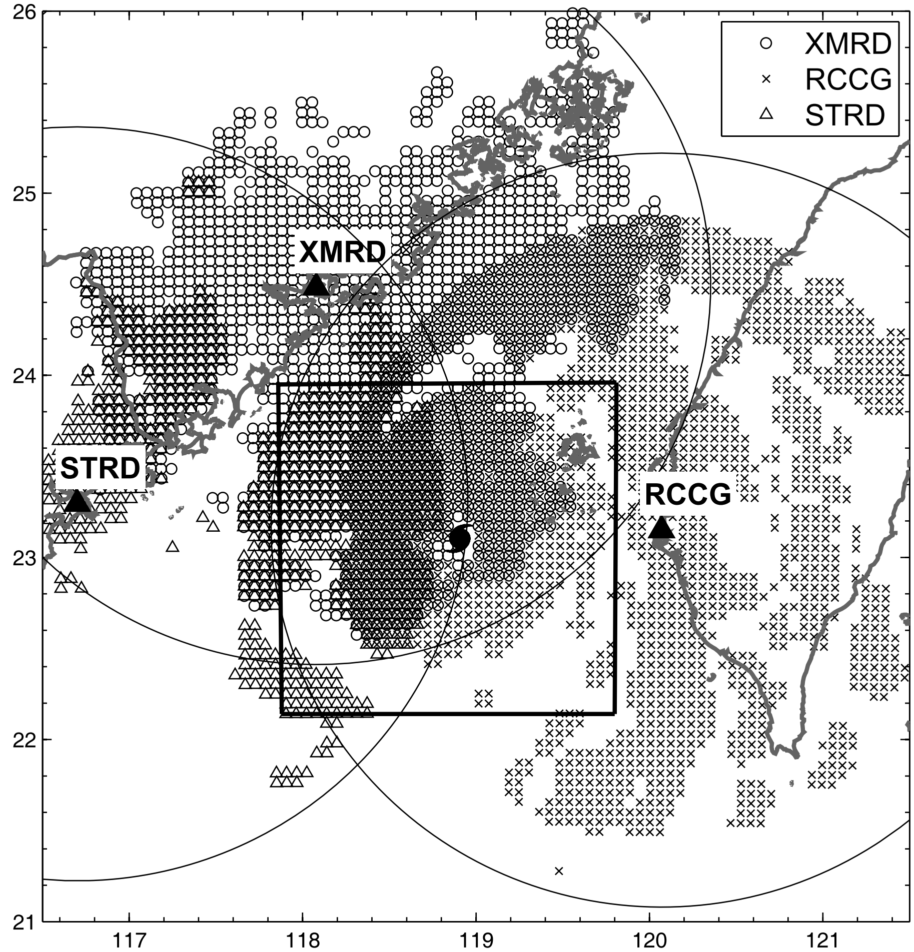

Figure 15. Valid Vr data points from Xiamen (XMRD) (open circle), Chi-Gu (RCCG) (cross), and Santou (STRD) (triangle) radars at the 3 km level at 12:00 UTC, 9 September , the time of first analysis. The thick box indicates the plotting domain shown in Figure 4b.

first analysis (Figure 4b). However, the wind increment vectors do not form a closed circulation around the center, and the nonradial component of wind is generally weak (RCCG radar is east of the plotting domain, in the direction of the thick dashed line in Figure 4b; see also Figure 1). The wind speed along the radar radial through the TC center (along the thick dashed line) is weaker than in ExpVZ (Figure 4a), due at least partly to the underestimation of cross-beam component. ExpVZ analyzes the flow field better because of the coverage by additional radars from different viewing angles (Figure 15).

[33] Because the wind analysis of ExpVZRCCG from the first analysis cycle is poorer than ExpVZ (Figures 4a and 4b), the increments of the second cycle are larger in ExpVZRCCG than in ExpVZ (Figures 4c and 4d). They become comparable from the third cycle onward (Figures 4e and 4f), indicating the establishment of vortex circulations of a similar quality after three analysis cycles, even when data from only one (well positioned) radar are used. To put it another way, ExpVZRCCG is able to build up dynamically consistent vortex-scale structure from single-Doppler data, but it takes more volume scans of data and assimilation cycles to achieve a comparable quality. With multiple radar coverage, wind fields can be analyzed quite accurately after a couple of cycles (but this is not necessarily true for all fields; compare Figure 3).

[34] At the end of the assimilation cycles, ExpVZ and ExpVZRCCG produce similar analyses in vortex structure, intensity and center location (Figure 13d). Their MSLPs (MSWs) are 983 hPa (33 m s^{-1}) and 984 hPa (32 m s^{-1}), respectively. With similar initial conditions, the predicted tracks (Figures 14a and 14b) and intensities (Figures 14c and 14d) in ExpVZRCCG and ExpVZ are similar, with those of ExpVZ being slightly better, especially in track and wind speed error during the later hours (Figures 14b and 14d).

[35] The weak mass continuity constraint in the ARPS 3DVAR does help significantly in improving the wind analysis. The constraint couples the three wind components together and helps to produce wind fields that approximately satisfy the mass continuity equation. An additional experiment was performed, which is the same as ExpVZRCCG, except that this constraint is turned off. Figure 16 shows the 3 km level flow analysis corresponding to Figure 4b. Without the constraint, the wind speed along the radial through the TC center is very weak, and most of the wind increments are in the radial direction.

[36] These results suggest that through several intermittent cycles assimilating data from a single well positioned radar,

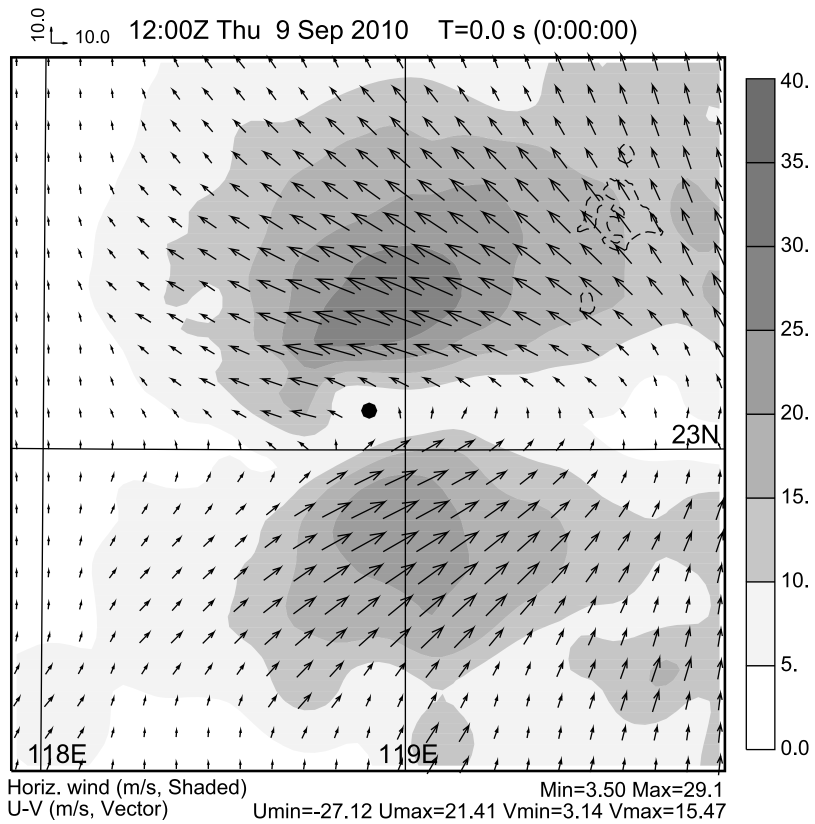

Figure 16. Same as Figure 4b but from an experiment that is the same as ExpVZRCCG but without the mass divergence constraint in ARPS 3DVAR.

using the ARPS 3DVAR with a mass continuity constraint, a quality circulation analysis of a typhoon can also be obtained. The use of more radars reduces the number of cycles needed to reach a similar quality. The forecasting results are somewhat better with multiple Doppler radars.

6. Summary and Conclusions

[37] This study examines, for the first time, the impact of intermittently assimilated high-resolution data of ground-based radars from Taiwan and mainland China, for the analysis and prediction of a typhoon making landfall on a 3 km high-resolution grid. This typhoon, Meranti (2010), intensified suddenly when it was near the southeast coast of China within the Taiwan Strait. The reflectivity (Z) and radial velocity (Vr) data from five S band coastal operational CINRAD WSR-98D radars from mainland China and three Gematronik 1500S Doppler radars from Taiwan were assimilated over a 6 h period (12:00 to 18:00 UTC) spanning the last 6 h of rapid intensification and about 1.5 h prior to landfall. The ARPS prediction model and its 3DVAR/cloud analysis system were used for intermittent assimilation cycles, which were followed by 12 h long predictions. Compared to similar studies published by these authors and others based on 3DVAR methods [e.g., *Xiao et al.*, 2007; *Zhao and Jin*, 2008; *Zhao and Xue*, 2009; *Lin et al.*, 2011], this study examines in more detail the analysis increments produced by the 3DVAR/cloud analysis system, the model responses during the forecast steps, the three dimensional structures of the analyzed typhoon, the effects of assimilation cycle lengths, the use of single versus multiple Doppler radars, and the amount and spatial distributions of precipitation after typhoon landfall. Direct verification against observations was performed whenever possible. Key results are summarized in the following paragraph.

[38] Experiments that only assimilate radar data over the 6 h long assimilation window produce final typhoon vortex analyses with maximum surface wind speeds that are very close to the best track data. The MSLP is up to 13 hPa too high, but it is much closer to the best track data than the operational NCEP GFS analysis, whose error is over 30 hPa. Because the ARPS 3DVAR system does not directly update pressure when analyzing radar data, the reduction in MSLP is achieved through model adjustments during the assimilation cycles, where pressure responds to the analyzed winds. The most significant improvement to the model vortex occurs in the first and second cycles, when the background error is larger. In later cycles, the corrections contain mostly subvortex, convective-scale structures. The center location and MSW are close to best track data; the axisymmetric wind and reflectivity structures of the analyzed typhoon also agree well with the radar-derived axisymmetric structures.

[39] With the improved initial conditions, the subsequent 12 h forecasts of typhoon structure, intensity, track and precipitation are greatly improved in all radar assimilation experiments. The improvement to both track and intensity predictions persists over the full 12 h forecast period. The

assimilation of Vr data is found to have a larger impact on the intensity and track than Z data, while additional Z data help to further improve the forecast precipitation structures. Overall, assimilating both Vr and Z at hourly intervals leads to the best forecast. With the improved track and structure forecasts of Typhoon Meranti, three local rainfall maxima related to typhoon circulations and their interaction with the complex terrain in Fujian province were captured well, except for small position errors and occasional under-prediction of rainfall amount.

[40] Sensitivity experiments suggest that the assimilation time interval also affects the analysis and forecast. The experiments with 3 and 6 hourly assimilation cycles predicted a somewhat weaker typhoon with larger track errors later on than the experiment with hourly cycles, but they still performed much better than the experiment without radar data. Assimilating MSLP from the best track in addition to radar resulted in a vortex whose MSLP is much closer to observed in the analysis, but the benefit was mostly lost within the first hour of free forecast, mainly because of the lack of balance between the pressure and temperature fields analyzed by the 3DVAR. A longer lasting benefit will require multivariate analysis methods that can produce a more balanced vortex. Assimilating data from a single Doppler radar with good coverage of the typhoon inner core region is also quite effective, except that it takes one more cycle to establish circulation analyses of a similar quality as the multiple radar case; although, the forecasts using multiple radars are still the best.

[41] We note finally that even though the conclusions drawn in this paper are based on a single case, detailed examinations of the analysis and forecasting results and processes lead us to believe that our results have general meaning, at least for the given or similar DA approaches used. Considering that radar DA research for tropical cyclone initialization is still relatively limited, our current study represents an important step toward eventual robust operational implementation of these techniques. In fact, a similar procedure is being tested in real time at CMA, and the evaluation of the system for many cases is the natural next step.

[42] **Acknowledgments.** This work was primarily supported by the Social Common Wealth Research Program (GYHY201006007), the National Fundamental Research 973 Program of China (2009CB421502), and the National Natural Science Foundation of China (grants 40975011, 40921160382, and 90815028) to the first and second authors. The third author was supported by the Office of Naval Research grants DOD-ONR N00014-10-1-0775 and N00014-10-1-0133 and by the National Thousand People Plan funding for his collaborative research at Nanjing University. We acknowledge the China Meteorological Administration and the P3 Mesoscale Research Lab in Taiwan University for collecting and archiving the radar data used in this study. Keith Brewster of CAPS, University of Oklahoma, provided assistance for the radar data quality control. Jordan Schleif helped proofread the paper. Y. Wang, J. Gao, G. Ge, N. Du, K. Zhu, and Q. Wang are thanked for help with ARPS and ARPS 3DVAR during the first author's visit to CAPS. Supercomputers at Nanjing University were used. Comments by Yi Jin and two anonymous reviewers improved the manuscript.

References

Atkinson, G. D., and C. R. Holliday (1977), Tropical cyclone minimum sea level pressure/maximum sustained wind relationship for western North Pacific, *Mon. Weather Rev.*, *105*, 421–427, doi:10.1175/1520-0493(1977)105<0421:TCMSLP>2.0.CO;2.

Brewster, K., M. Hu, M. Xue, and J. Gao (2005), Efficient assimilation of radar data at high resolution for short-range numerical weather prediction, paper presented at International Symposium on Nowcasting and Very Short Range Forecasting, World Weather Res. Prog., Toulouse, France, 5–9 Sep.

Chen, Y., and C. Snyder (2007), Assimilating vortex position with an ensemble Kalman filter, *Mon. Weather Rev.*, *135*, 1828–1845, doi:10.1175/MWR3351.1.

Crum, T. D., R. L. Albert, and D. W. Burgess (1993), Recording, archiving, and using WSR-88D data, *Bull. Am. Meteorol. Soc.*, *74*, 645–653, doi:10.1175/1520-0477(1993)074<0645:RAAUWD>2.0.CO;2.

Davis, C., et al. (2008), Prediction of landfalling hurricanes with the Advanced Hurricane WRF model, *Mon. Weather Rev.*, *136*, 1990–2005, doi:10.1175/2007MWR2085.1.

Dong, J., and M. Xue (2010), Ensemble Kalman filter assimilation of coastal WSR-88D radar data and forecasting for Hurricane Ike (2008), paper presented at 29th Conference on Hurricanes and Tropical Meteorology, Am. Meteor. Soc., Tucson, Ariz., 10–14 May.

Doviak, R. J., P. S. Ray, R. G. Stauch, and L. J. Miller (1976), Error estimation in wind fields derived from dual-Doppler radar measurement, *J. Appl. Meteorol.*, *8*, 249–253.

Dowell, D., F. Zhang, L. J. Wicker, C. Snyder, and N. A. Crook (2004), Wind and temperature retrievals in the 17 May 1981 Arcadia, Oklahoma, supercell: Ensemble Kalman filter experiments, *Mon. Weather Rev.*, *132*, 1982–2005, doi:10.1175/1520-0493(2004)132<1982:WATRIT>2.0.CO;2.

Evensen, G. (2003), The ensemble Kalman filter: Theoretical formulation and practical implementation, *Ocean Dyn.*, *53*, 343–367, doi:10.1007/s10236-003-0036-9.

Gao, J. D., M. Xue, A. Shapiro, and K. K. Droegemeier (1999), A variational method for the analysis of three-dimensional wind fields from two Doppler radars, *Mon. Weather Rev.*, *127*, 2128–2142, doi:10.1175/1520-0493(1999)127<2128:AVMFTA>2.0.CO;2.

Gao, J. D., M. Xue, K. Brewster, and K. K. Droegemeier (2004), A three-dimensional variational data analysis method with recursive filter for Doppler radars, *J. Atmos. Oceanic Technol.*, *21*, 457–469, doi:10.1175/1520-0426(2004)021<0457:ATVDAM>2.0.CO;2.

Hamill, T. M., J. S. Whitaker, M. Fiorino, and S. G. Benjamin (2011), Global ensemble predictions of 2009's tropical cyclones initialized with an ensemble Kalman filter, *Mon. Weather Rev.*, *139*, 668–688, doi:10.1175/2010MWR3456.1.

Harasti, P. R., C. J. McAdie, P. P. Dodge, W. C. Lee, J. Tuttle, S. T. Murillo, and F. D. Marks (2004), Real-time implementation of single-Doppler radar analysis methods for tropical cyclones: Algorithm improvements and use with WSR-88D display data, *Weather Forecast.*, *19*, 219–239, doi:10.1175/1520-0434(2004)019<0219:RIOSRA>2.0.CO;2.

Hendricks, E. A., J. R. Moskaitis, Y. Jin, R. M. Hodur, J. D. Doyle, and M. S. Peng (2011), Prediction and diagnosis of Typhoon Morakot (2009) using the Naval Research Laboratory's mesoscale tropical cyclone model, *Terr. Atmos. Oceanic Sci.*, *22*, 579–594, doi:10.3319/TAO.2011.05.30.01(TM).

Houze, R. A., Jr., S. S. Chen, B. F. Smull, W. C. Lee, and M. M. Bell (2007), Hurricane intensity and eye wall replacement, *Science*, *315*, 1235–1239, doi:10.1126/science.1135650.

Hu, M., and M. Xue (2007), Impact of configurations of rapid intermittent assimilation of WSR-88D radar data for the 8 May 2003 Oklahoma City tornadic thunderstorm case, *Mon. Weather Rev.*, *135*, 507–525, doi:10.1175/MWR3313.1.

Hu, M., M. Xue, and K. Brewster (2006a), 3DVAR and cloud analysis with WSR-88D level-II data for the prediction of Fort Worth tornadic thunderstorms. Part I: Cloud analysis and its impact, *Mon. Weather Rev.*, *134*, 675–698, doi:10.1175/MWR3092.1.

Hu, M., M. Xue, J. Gao, and K. Brewster (2006b), 3DVAR and cloud analysis with WSR-88D level-II data for the prediction of Fort Worth tornadic thunderstorms. Part II: Impact of radial velocity analysis via 3DVAR, *Mon. Weather Rev.*, *134*, 699–721, doi:10.1175/MWR3093.1.

Kalnay, E. (2003), *Atmospheric Modeling, Data Assimilation, and Predictability*, 341pp., Cambridge Univ. Press, Cambridge, U. K.

Kessler, E. (1969), *On the Distribution and Continuity of Water Substance in Atmospheric Circulations*, *Meteorol. Monogr.*, vol. 10, 84pp., Am. Meteorol. Soc., Boston, Mass.

Lee, W.-C., and M. M. Bell (2007), Rapid intensification, eye wall contraction, and breakdown of Hurricane Charley (2004) near landfall, *Geophys. Res. Lett.*, *34*, L02802, doi:10.1029/2006GL027889.

Lee, W.-C., B. J.-D. Jou, P.-L. Chang, and S. M. Deng (1999), Tropical cyclone kinematic structure retrieved from single-Doppler radar observations. Part I: Interpretation of Doppler velocity patterns and the GBVTD technique, *Mon. Weather Rev.*, *127*, 2419–2439, doi:10.1175/1520-0493(1999)127<2419:TCKSRF>2.0.CO;2.

Lee, W.-C., B. J.-D. Jou, P.-L. Chang, and F. D. Marks Jr. (2000), Tropical cyclone kinematic structure retrieved from single-Doppler radar observations. Part III: Evolution and structures of Typhoon Alex (1987), *Mon.*

Weather Rev., *128*, 3982–4001, doi:10.1175/1520-0493(2000)129<3982:TCKSRF>2.0.CO;2.

Lin, H. H., P. L. Lin, Q. N. Xiao, and Y. H. Kuo (2011), Effect of Doppler radial velocity data assimilation on the simulation of a typhoon approaching Taiwan: A case study of Typhoon Aere (2004), *Terr. Atmos. Oceanic Sci.*, *22*(3), 325–345, doi:10.3319/TAO.2010.10.08.01(A).

Liu, Y., D.-L. Zhang, and M. K. Yau (1999), A multiscale numerical study of Hurricane Andrew (1992). Part II: Kinematics and inner-core structures, *Mon. Weather Rev.*, *127*, 2597–2616, doi:10.1175/1520-0493(1999)127<2597:AMNSOH>2.0.CO;2.

Oye, R., C. Mueller, and C. Smith (1995), Software for radar data translation, visualization, editing, and interpolation, in *27th Conference on Radar Meteorology*, pp. 359–361, Am. Meteorol. Soc., Boston, Mass.

Rogers, R. R., and M. K. Yau (1989), *A Short Course in Cloud Physics*, 3rd ed., 293 pp., Pergamon, Oxford, U. K.

Schaefer, J. T. (1990), The critical success index as an indicator of warning skill, *Weather Forecasting*, *5*, 570–575, doi:10.1175/1520-0434(1990)005<0570:TCSIAA>2.0.CO;2.

Schenkman, A. D., M. Xue, A. Shapiro, K. Brewster, and J. Gao (2011), The analysis and prediction of the 8–9 May 2007 Oklahoma tornadic mesoscale convective system by assimilating WSR-88D and CASA radar data using 3DVAR, *Mon. Weather Rev.*, *139*, 224–246, doi:10.1175/2010MWR3336.1.

Tong, M., and M. Xue (2005), Ensemble Kalman filter assimilation of Doppler radar data with a compressible nonhydrostatic model: OSS experiments, *Mon. Weather Rev.*, *133*, 1789–1807, doi:10.1175/MWR2898.1.

Xiao, Q., and J. Sun (2007), Multiple radar data assimilation and short-range quantitative precipitation forecasting of a squall line observed during IHOP_2002, *Mon. Weather Rev.*, *135*, 3381–3404, doi:10.1175/MWR3471.1.

Xiao, Q., Y. H. Kuo, J. Sun, W. C. Lee, D. M. Barker, and E. Lim (2007), An approach of radar reflectivity data assimilation and its assessment with the inland QPF of Typhoon Rusa (2002) at landfall, *J. Appl. Meteorol. Climatol.*, *46*, 14–22, doi:10.1175/JAM2439.1.

Xue, M., K. K. Droegemeier, and V. Wong (2000), The Advanced Regional Prediction System (ARPS)—A multi-scale nonhydrostatic atmospheric simulation and prediction tool. Part I: Model dynamics and verification, *Meteorol. Atmos. Phys.*, *75*, 161–193, doi:10.1007/s007030070003.

Xue, M., K. K. Droegemeier, V. Wong, A. Shapiro, K. Brewster, F. Carr, D. Weber, Y. Liu, and D.-H. Wang (2001), The Advanced Regional Prediction System (ARPS)—A multi-scale nonhydrostatic atmospheric simulation and prediction tool. Part II: Model physics and applications, *Meteorol. Atmos. Phys.*, *76*, 143–165, doi:10.1007/s007030170027.

Xue, M., D. H. Wang, J. D. Gao, K. Brewster, and K. K. Droegemeier (2003), The Advanced Regional Prediction System (ARPS), storm-scale numerical weather prediction and data assimilation, *Meteorol. Atmos. Phys.*, *82*(1–4), 139–170, doi:10.1007/s00703-001-0595-6.

Yu, H., C. Hu, and L. Jiang (2007), Comparison of three tropical cyclone intensity datasets, *Acta Meteorol. Sin.*, *21*, 121–128.

Zhang, F., Y. Weng, J. A. Sippel, Z. Meng, and C. H. Bishop (2009), Cloud-resolving hurricane initialization and prediction through assimilation of Doppler radar observations with an ensemble Kalman filter, *Mon. Weather Rev.*, *137*, 2105–2125, doi:10.1175/2009MWR2645.1.

Zhao, K., and M. Xue (2009), Assimilation of coastal Doppler radar data with the ARPS 3DVAR and cloud analysis for the prediction of Hurricane Ike (2008), *Geophys. Res. Lett.*, *36*, L12803, doi:10.1029/2009GL038658.

Zhao, Q., and Y. Jin (2008), High-resolution radar data assimilation for Hurricane Isabel (2003) at landfall, *Bull. Am. Meteorol. Soc.*, *89*, 1355–1372, doi:10.1175/2008BAMS2562.1.

Zhao, Q., J. Cook, Q. Xu, and P. R. Harasti (2008), Improving short-term storm predictions by assimilating both radar radial-wind and reflectivity observations, *Weather Forecasting*, *23*, 373–391, doi:10.1175/2007WAF2007038.1.

B. J.-D. Jou, Department of Atmospheric Sciences, National Taiwan University, Taipei 10600, Taiwan.

W.-C. Lee, Earth Observing Laboratory, National Center for Atmospheric Research, Boulder, CO 80307, USA.

X. Li, M. Xue, and K. Zhao, Key Laboratory of Mesoscale Severe Weather/MOE, School of Atmospheric Sciences, Nanjing University, Nanjing 210093, China. (zhaokun@nju.edu.cn)